Diese Arbeit wurde vorgelegt am
Lehr- und Forschungsgebiet Theorie der hybriden Systeme

Optimales Design und Scheduling einer Smart City unter unsicherer erneuerbarer Energieerzeugung

Optimal Design and Scheduling of a Smart City Under Uncertain Renewable Energy Generation

Masterarbeit
Informatik

Juli 2021

Vorgelegt von Presented by	Christoph von Oy Schulstraße 14 52477 Alsdorf Matrikelnummer: 356414 christoph.von.oy@rwth-aachen.de
Erstprüfer First examiner	Prof. Dr. rer. nat. Erika Ábrahám Lehr- und Forschungsgebiet: Theorie der hybriden Systeme RWTH Aachen University
Zweitprüfer Second examiner	Prof. Sebastian Krumscheid, Ph.D. Chair of Mathematics for Uncertainty Quantification RWTH Aachen University
Fachlicher Betreuer Professional supervisor	Dr. rer. nat. Pascal Richter Lehr- und Forschungsgebiet: Theorie der hybriden Systeme RWTH Aachen University
Externer Betreuer External supervisor	Sonja Germscheid, M.Sc. Institut für Energie- und Klimaforschung: Modellierung von Energiesystemen Forschungszentrum Jülich

Eigenständigkeitserklärung

Hiermit versichere ich, dass ich diese Mastararbeit selbständig verfasst und keine anderen als die angegebenen Quellen und Hilfsmittel benutzt habe. Die Stellen meiner Arbeit, die dem Wortlaut oder dem Sinn nach anderen Werken entnommen sind, habe ich in jedem Fall unter Angabe der Quelle als Entlehnung kenntlich gemacht. Dasselbe gilt sinngemäß für Tabellen und Abbildungen. Diese Arbeit hat in dieser oder einer ähnlichen Form noch nicht im Rahmen einer anderen Prüfung vorgelegen.

Aachen, im Juli 2021

Christoph von Oy

Abstract

Increasing the share of renewable energy while maintaining a high degree of self-sufficiency is a major challenge within energy system design for cities. This work uses a two-stage stochastic program, formulated as a mixed integer linear program to optimise the energy system of a city under additional constrains of self sufficiency. Multiple uncertainties have to be addressed during optimal design of energy systems. Energy production from solar and wind power as well as energy demand are considered uncertain. A technique aggregating historical data into typical periods is used for scenario generation. Using a case study of a city in western Germany, the effects of either using typical days or typical weeks during scenario generation and different self-sufficiency enforcing strategies and levels on the resulting optimal design were examined. Longer typical periods seem to increase the flexibility in the operating schedule regarding storage components. With more aggressive strategies and higher levels of self-sufficiency, we observe a displacement of varying and uncertain energy sources by stable and deterministic ones.

Contents

Nomenclature

Sets and indices

$k \in K$	Power producing components $\{\mathrm{pv}, \mathrm{wind}, \mathrm{biogas}, \mathrm{hydro}\}$
$l \in L$	Energy storing components $\{\mathrm{pump}, \mathrm{h}, \mathrm{ch4}, \mathrm{bat}\}$
$i \in L \cup K$	Power producing and energy storing components
$s \in S$	Scenario s in set of scenarios S
$t \in T$	Time step t in time series T

Variable	**Description**	**Unit**	**Type**
$APVF_{\mathrm{i}}$	Annual present value factor for component i	1/a	Parameter
C	Total additional costs	€/a	Objective
$E(C)$	Expected total additional costs	€/a	Objective
$C_{\mathrm{grid},s,t}$	Additional costs	€	Objective
I	Total annualised investment costs	€/a	Objective
I_{i}	Investment costs of component i	€	Objective
M	Total maintenance costs	€/a	Objective
M_{i}	Maintenance costs of component i	€/a	Objective
N_{wind}	Number of wind turbines	-	Design
$P_{\mathrm{biogas,N}}$	Installed CHP capacity for the biogas component	kW	Design
$P_{\mathrm{biogas,N,add}}$	Additional CHP capacity for the biogas component	kW	Design
$P_{\mathrm{buy},s,t}$	Purchased energy from the external grid	kW	Operation
$P_{\mathrm{demand},s,t}$	Consumed energy by the consumption component	kW	Operation
$P_{\mathrm{hydro,N}}$	Installed capacity for the hydroelectric component	kW	Design
$P_{\mathrm{k},s,t}$	Produced power by component k	kW	Operation
$P_{\mathrm{l,char,N}}$	Installed charging capacity for component l	kW	Design
$P_{\mathrm{l,char},s,t}$	Consumed power by charging of component l	kW	Operation
$P_{\mathrm{l,dis,N}}$	Installed discharging capacity for component l	kW	Design
$P_{\mathrm{l,dis},s,t}$	Produced power by discharging of component l	kW	Operation
$P_{\mathrm{sell},s,t}$	Sold energy to the external grid	kW	Operation
$P_{\mathrm{pv,N,farm}}$	Installed capacity of solar farms	kW	Design
$P_{\mathrm{pv,N,roof}}$	Installed capacity of rooftop installations	kW	Design
$Q_{\mathrm{l,N}}$	Storage capacity of component l	kWh	Design
$Q_{\mathrm{l},s,t}$	Stored amount of energy in component l	kWh	Operation
TAC	Total expected annual system cost	€/a	Objective
$V_{\mathrm{biogas,N}}$	Storage capacity of biogas storage	m^3	Design
$V_{\mathrm{biogas},s,t}$	Stored amount of gas in biogas storage	m^3	Operation
Var^{max}	Upper bound for a generic variable Var	-	-
a_i	Economic lifetime of component i	a	Parameter
c_{buy}	Electricity tariff	€/kWh	Parameter
c_{sell}	Feed-in tariff	€/kWh	Parameter
f	Self-sufficiency factor	-	Parameter
n_{period}	Number of times a typical period fits into a year	1/a	Parameter
n_s	Weight of scenario s	1/a	Parameter
$p_{\mathrm{pv},s,t}$	Specific capacity of the photovoltaic component	-	Parameter
$p_{\mathrm{wind},s,t}$	Specific capacity of the wind component	kW	Parameter
$q_{\mathrm{bat,max}}$	Maximal depth of discharge	-	Parameter
r	Interest rate	-	Parameter
Δt	Length of one time step	h	Parameter

$\eta_{\mathrm{l,char}}$	Charging efficiency of component l	-	Parameter
$\eta_{\mathrm{l,dis}}$	Discharging efficiency of component l	-	Parameter
$\eta_{\mathrm{l,self}}$	Self-discharging rate of component l	-	Parameter
π_s	Probability of scenario s	-	Parameter

1. Introduction

Global carbon emissions are rising, cf. Figure 1.1, causing a rise in atmospheric temperature, which has severe effects on the environment like loss of biodiversity and an increased frequency of natural disasters [31].

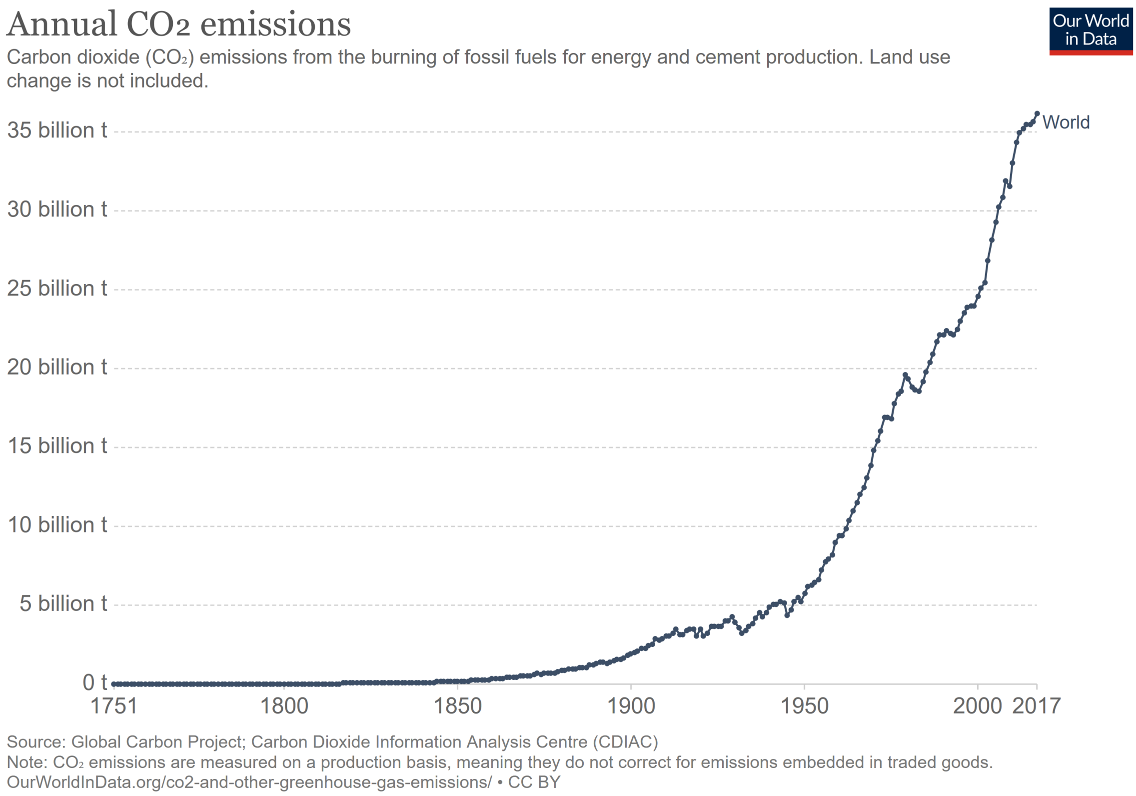

Figure 1.1: Annual carbon emissions [53].
Since the beginning of the 20th century, annual carbon emissions have been increasing exponentially, leading to a severe increase of atmospheric temperature, frequency of natural disasters and loss of biodiversity.

57 % of green house gas emissions are caused by energy production for industry and electricity [52]. Reducing shares of high carbon energy sources like coal can help to bring down carbon emissions significantly. Increasing energy production from low carbon, renewable sources is needed to close the gap in production. Therefore the EU [14] as well as the German government [11] have introduced goals to increase the market shares of renewable energy sources.

Solar power is readily available, enough to theoretically fulfil the energy demands of the entire world [33]. But its supply is fluctuating and not known far in advance. Other renewable energy sources like wind and hydroelectricity also face uncertainty in their power output. Storage technologies need to be included to guarantee supply security, by storing excessive energy from sunny days for night hours or days with unexpected high demand. Diversifying energy sources, taking uncertainty into account and including storage technologies are essential when trying to meet renewable energy targets.

Another impeding factor for the widespread adoption of renewable energy is its high cost, compared to traditional non-renewable technologies. Technological innovation and economy of scale can bring down such costs. However, factoring in the price of different renewable technologies when designing a diverse energy system, can guide the design process to select the most low cost combination of renewable technologies. This can bring down the cost of renewable energy without the need to wait for future cost reduction via technological innovation. Choosing cost reduction as a prime objective during design of energy systems can minimise costs and therefore facilitate the transition to renewable energy.

Besides a variability in time, the availability of renewable energy varies from location to location. Large transmission lines that bring renewable energy from wind and sun rich areas to other parts of the country are needed. High costs and long planning times for transmission lines present challenges for renewable energy. Full or partial self-sufficiency on a per city basis, by producing electricity locally, mitigates the need for large transmission lines.

With the above-mentioned challenges and advantages, designing an energy system that is diverse, uses storage and produces energy locally for local consumption can aid in the transition to renewable energy. Such a system is called a distributed energy system (DES), and a city that utilises such a DES is called a smart city. This work develops a method for designing a DES for a city under the uncertainty of electricity demand and available power. The method incorporates the goal of self-sufficiency while keeping the cost of the DES as low as possible.

1.1. State of the Art

Designing a DES under constraints of self-sufficiency while minimising its cost can be formulated as an optimisation problem. The nature of an optimisation problem is to find solutions for a set of decisions that optimises a given objective function [42]. Additionally, the decisions are subject to a set of constraints.

In the case of DES design, the decisions mainly consist of selecting what technologies should be used and what their installed capacities inside the system should be. The constraints capture the behaviour and technical restrictions of the DES, as well as additional constraints like available resources and special design goals like self-sufficiency. The objective function evaluates the DES design and is most commonly of an economic nature, but can also incorporate environmental factors like the designs carbon footprint.

It is also important to include the operation of the DES. During operation a schedule for the DES has to be decided. The schedule dictates which components are switched on, at what part loads each component operates, or how much energy is charged or discharged into storage components. These operational decisions can influence the overall costs, for example overproduced energy can be sold for revenue. Furthermore, constraints like self-sufficiency can only be enforced during system operation. Therefore the consideration of possible operating schedules in design optimisation is imperative.

The problem of facing uncertainty during optimisation can be tackled by using stochastic programming [9]. In a stochastic program, some parameters are considered uncertain. Only probability descriptions are known, most often as probability distributions. These distributions are discretised into a finite set of scenarios, each with its own probability. The goal of the stochastic program is to find a solution that is feasible for all possible scenarios and optimises the expected value of the objective function.

Stochastic programming presents two challenges. First, accurate representations of the considered uncertainty using scenarios have to be determined. Second, solving the resulting stochastic program. If the constraints and objective function of a stochastic program are linear, it can be expressed as a linear program (LP). If some decisions, like the number of wind turbines, can only be integers, the problem is a mixed integer linear program (MILP). A host of solvers and algorithms for MILP optimisation problems exist, which are able to find optimal solutions for complex problems. Additionally, special algorithms for solving MILP formulations of stochastic programs exist that can take advantage of its underlying structure, like Bender Decomposition [8].

Using stochastic programming to design an optimal DES under uncertainty has been adopted by several authors, e.g., [45, 60, 58]. Other techniques include robust optimisation [5, 6]. Regarding the objective function all works employ an objective function that minimises costs. Wang et al. [58] use multi-objective optimisation to optimise for cost and carbon footprint, whereas Mavromatidis et al. [45] enforce low carbon emissions using constraints without optimising them.

In the following we provide a small overview of several aspects from the above cited works. Various parameters can be considered uncertain. All energy demands that the DES should supply, usually electricity, heating and cooling, are considered uncertain. When renewable energy sources like solar and wind power are incorporated into the DES, their availability is also considered uncertain. The majority also view energy carrier prices, for electricity, biomass and gas as uncertain. Mavromatidis et al. [45] additionally regard the grid emission factor, the amount of CO_2 released per unit of purchased electricity, as uncertain. Compared to optimisation under uncertainty, deterministic optimisation tend to find optimal DES designs with smaller unit sizes and capacities. This arises from the fact that extreme scenarios with peak demand and low supply are usually not represented in deterministic optimisations. Optimisation under uncertainty can account for such extreme events, leading to designs that are guaranteed to function during extreme events, necessitating larger unit sizes. The costs of designs under uncertainty are higher, largely due to larger investment costs from larger unit sizes.

Mavromatidis et al. [47] use global sensitivity analysis to investigate which uncertain factors have the largest impact on the economic performance of a DES. Parameters analysed are energy carrier prices, emission factors, investment costs and technical characteristics of technologies used in the DES, energy demand and solar radiation patterns. Uncertainties in energy demand patterns and energy carrier prices have the largest impact on the costs of a DES. Investment costs and technical characteristics have minimal impact.

Besides DES design, stochastic programming can also be used to optimise the operation of an existing DES under uncertainty, e.g., [18, 44]. For a given DES, operational decisions have to be made, usually modelled on a daily basis. Di Somma et al. [18] optimise for low cost and carbon emissions in a DES for a residential building. Schedules computed under uncertainty can reduce costs and carbon emissions due to better utilisation of the available DES resources. Marino et al. [44] minimise operational costs of a DES for a medium sized college in San Francisco. Additional constraints are used to enforce higher utilisation of installed photovoltaic panels within the DES. With higher utilisation, lower system costs are observed. As with DES design, energy demand is considered uncertain in both works. Additionally, energy prices and solar irradiation can be considered uncertain.

1.2. Outline

In the above cited literature, approaches for optimising the design or operation of DES under uncertainty are presented. These approaches are usually examined using case studies of small neighbourhoods or single buildings like universities or hospitals. The additional design goal of self-sufficiency is not considered. To design a DES for a city under the uncertainty of electricity demand and available power, the presented optimisation approaches have to be adapted to DES of larger scales. This involves incorporating power generation and energy storage technologies into the optimisation problem that can only be utilised on a city or regional level, like hydroelectricity. Additionally, suitable methods for incorporating self-sufficiency into the design goals are needed. This work focuses on contributing to both challenges, large scale DES design for a city, and incorporating self-sufficiency. In Section 2, a mathematical model, describing of behaviour of a DES is developed. In Section 3, the mathematical model is translated into a deterministic optimisation program We specify an objective function and provide additional constraints that guarantee a desired level of self-sufficiency and express design limitations. The deterministic program is expanded into a two-stage stochastic program in Section 4. First we discuss, which parameters are considered uncertain. Then we extend the deterministic model into a two-stage stochastic program. The uncertainty of unknown parameters is quantified by computing sets of representative periods from historical data. In a case study in Section 5, the developed stochastic model is used to design a DES for a German city. We compare the effect of using representative periods of different length in the uncertainty quantification on optimal DES designs. We also analyse the impact of different self-sufficiency strategies on optimal DES designs. In the end, Section 6 concludes by discussing the results and giving an outlook on future work.

2. Model

In this section, a mathematical model describing the characteristics of a DES is developed. In Section 2.1, the structure of the model is discussed. In Section 2.2, we model the power generating technologies, and in Section 2.3 the storage technologies. The development of the model is finished in Sections 2.4 and 2.5 with additional model components that connect the DES to an external energy grid and to the smart city.

2.1. Model Structure

In this work, we focus on a DES that supplies electricity to a city. The goal is to reach a high degree of self-sufficiency, using only renewable energy sources. Figure 2.1 shows the structure of the DES. We model four renewable power generation technologies: photovoltaic power, wind power, biogas plants and hydroelectricity. As energy storage is essential for a DES, we model four energy storage technologies: pumped hydropower, hydrogen storage, Power-to-Gas (PTG) storage and battery storage. Each technology is represented by a component in the model structure. The city, the consumer of the produced electricity, is modelled in the consumption component. A connection to the national electric grid is represented by the connection component. The components are connected using a single bus, representing the local electricity grid. We neglect transmission losses within the local electricity grid and consider the transmission infrastructure given, i.e., we do not have to model and optimise the transmission infrastructure.

In the following, the upfront investment costs, yearly operations and maintenance costs, and additional costs or all modules are introduced, as they are used in the definition of the objective function, see Section 3.2.

2.2. Renewable Power Plants

In this section we model four different renewable energy sources. Photovoltaic (PV) modules, converting solar irradiation to electricity, see Section 2.2.1, wind turbines, harnessing energy from wind, see Section 2.2.2, biogas plants, digesting organic matter into biogas, see Section 2.2.3, and hydroelectricity, harnessing the flow of water, see Section 2.2.4.

2.2.1. Photovoltaic Component

A photovoltaic module generates electric power from sunlight. The capacity of a solar installation can either be measured by the total area of all installed PV modules or by the installed peak capacity. In the literature, the investment costs of solar installations are usually given for the installed peak capacity and not for the installed area [36, 49, 24]. Therefore, the peak capacity measure is used in the following.

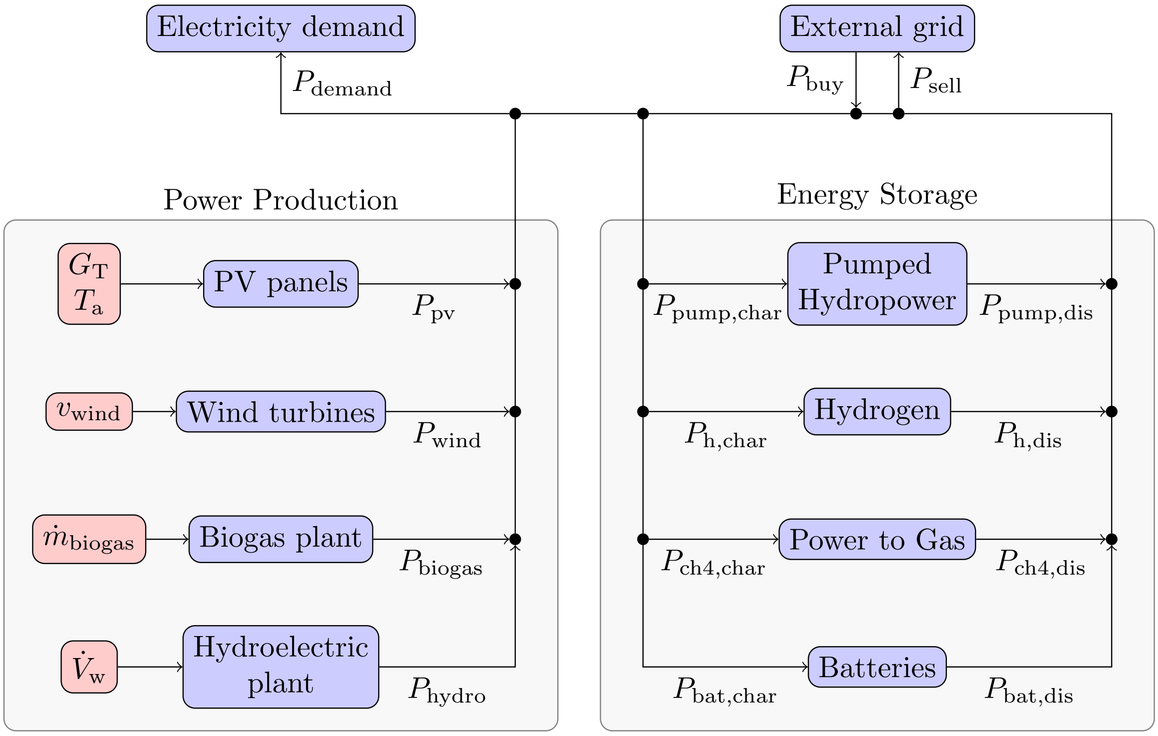

Figure 2.1: Block diagram of the DES.
On the left, the four power producing components are grouped together. The model parameters determining their power output are shown in red. On the right, the energy storage components are grouped together. The connection to an external electricity grid is represented by the external grid component. The smart city, the main consumer of the electricity provided by the DES, is represented by the electricity demand component.

The generated power P_{pv} can be computed by

$$P_{\mathrm{pv}} = P_{\mathrm{pv,N}} \cdot \eta_{\mathrm{pv}} \cdot \frac{G_{\mathrm{T}}}{G_{\mathrm{ref}}}, \tag{2.1}$$

where $P_{\mathrm{pv,N}}$ is the peak capacity, η_{pv} the influence of temperature on the electric efficiency of the module, G_{T} the total solar irradiation, and G_{ref} the reference solar irradiation, provided by the module manufacturer [55].

The traditional relation for the temperature influence is linear

$$\eta_{\mathrm{pv}} = 1 - \beta_{\mathrm{ref}} \cdot (T_{\mathrm{c}} - T_{\mathrm{ref}}), \tag{2.2}$$

where β_{ref} is the temperature dependence of the PV module and T_{ref} the reference cell temperature [55]. Both values are module dependant and provided by the manufacturer.

Often the operating cell temperature T_{c} is not available. Skoplaki and Palyvos [55] approximate T_{c} using the nominal operating cell temperature T_{NOCT}, measured un-

Installed peak capacity	**Investment cost**	**Source**
10 kW	1300 €/kW	[36]
55 kW	1112.5 €/kW	[24]
500 kW	900 €/kW	[36]
750 kW	950 €/kW	[49]
2 MW	700 €/kW	[36]
2 MW	800 €/kW	[49]
10 MW	700 €/kW	[49]

Table 2.1: Specific investment costs of photovoltaic power systems.
With increasing installed peak capacity a decrease of investment cost per kW can be observed.

der standardised conditions, and adjusting it using the total solar irradiance G_{T} and ambient temperature T_{a}. This results in the equation

$$\eta_{\mathrm{pv}} = \left(1 - \beta_{\mathrm{ref}} \cdot \left(T_{\mathrm{a}} - T_{\mathrm{ref}} + (T_{\mathrm{NOCT}} - T_{\mathrm{a}}) \cdot \frac{G_{\mathrm{T}}}{G_{\mathrm{NOCT}}}\right)\right). \tag{2.3}$$

The nominal irradiance G_{NOCT} is standardised to $800\,\mathrm{W/m^2}$. The nominal operating cell temperature T_{NOCT} is module dependant and provided by the manufacturer. See Appendix A.2 for the computation of the total solar irradiation G_{T}.

Figure 2.2 gives a schematic representation of the photovoltaic component with its inputs and outputs.

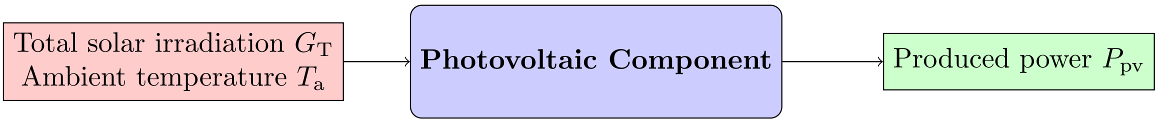

Figure 2.2: Block diagram of the photovoltaic component.
The total solar irradiation and ambient temperature are model inputs and the produced power is a model output of the photovoltaic component.

Considering the investment costs of a PV power plant, Table 2.1 shows that smaller scale plants are considerably more expensive per kW installed peak capacity than larger ones. A contributor to this effect is the fact that smaller PV plants are usually installed on residential or commercial rooftops, and large-scale plants, called solar farms, are installed on dedicated pieces of land, reducing construction costs [36].

Regarding the goal of designing a cost efficient energy system it would be beneficial to only use large scale PV plants. However, such plants are restricted by the available land area. In use cases with limited available land, a large number of smaller scaled rooftop plants could be considered.

In order to account for both variants, the computation of the investment and maintenance costs is split into two parts. Both variants have their own installed peak capacity,

Parameter	Value
$i_{\text{pv,roof}}$	1000 €/kW
$i_{\text{pv,farm}}$	750 €/kW
$m_{\text{pv,roof}}$	10 €/(kW a)
$m_{\text{pv,farm}}$	15 €/(kW a)

Table 2.2: Specific investment and maintenance costs for the photovoltaic component. The specific costs are adapted from [36, 24, 49].

$P_{\text{pv,N,roof}}$ for rooftop installations, and $P_{\text{pv,N,farm}}$ for solar farms. Together they add up to the peak capacity of the PV component

$$P_{\text{pv,N}} = P_{\text{pv,N,roof}} + P_{\text{pv,N,farm}}. \tag{2.4}$$

Similar to [36] the specific investment costs listed in Table 2.1 are split into rooftop installations and solar farms based on the installed peak capacity. Plants below 1 MW are classified as rooftop installations, plants above 1 MW as solar farms. Specific investment costs of 1000 €/kW are chosen for rooftop installations, and 750 €/kW for solar farms, based on the average of the values from Table 2.1.

Maintenance costs of PV plants are 1 % of investment costs for small-scale rooftops installations [59] and 2 % for solar farms [49].

The investment costs of the PV component I_{pv} can now be computed by

$$I_{\text{pv}} = P_{\text{pv,N,roof}} \cdot i_{\text{pv,roof}} + P_{\text{pv,N,farm}} \cdot i_{\text{pv,farm}}, \tag{2.5}$$

and the maintenance costs M_{pv} by

$$M_{\text{pv}} = P_{\text{pv,N,roof}} \cdot m_{\text{pv,roof}} + P_{\text{pv,N,farm}} \cdot m_{\text{pv,farm}} \tag{2.6}$$

with the specific investment and maintenance costs listed in Table 2.2.

2.2.2. Wind Component

A wind turbine generates electric energy from wind energy. The generated power of a single wind turbine P_{wind} can be computed using the performance curve method

$$P_{\text{wind}} = p_{\text{power}}(v_{\text{wind,hub}}), \tag{2.7}$$

where $v_{\text{wind,hub}}$ is the wind speed measured at hub height and $p_{\text{power}}(-)$ the performance curve.

The performance curve is turbine dependant and provided by the manufacturer. In our model, we use a generic wind turbine, with a generic performance curve. The generic performance curve is derived by combining performance curves from multiple turbines models, based on an approach from Bahl et al. [7].

Figure 2.3a shows performance curves from four different turbine models. Each curve is defined over a set range of wind speeds. For wind speeds below this range, the

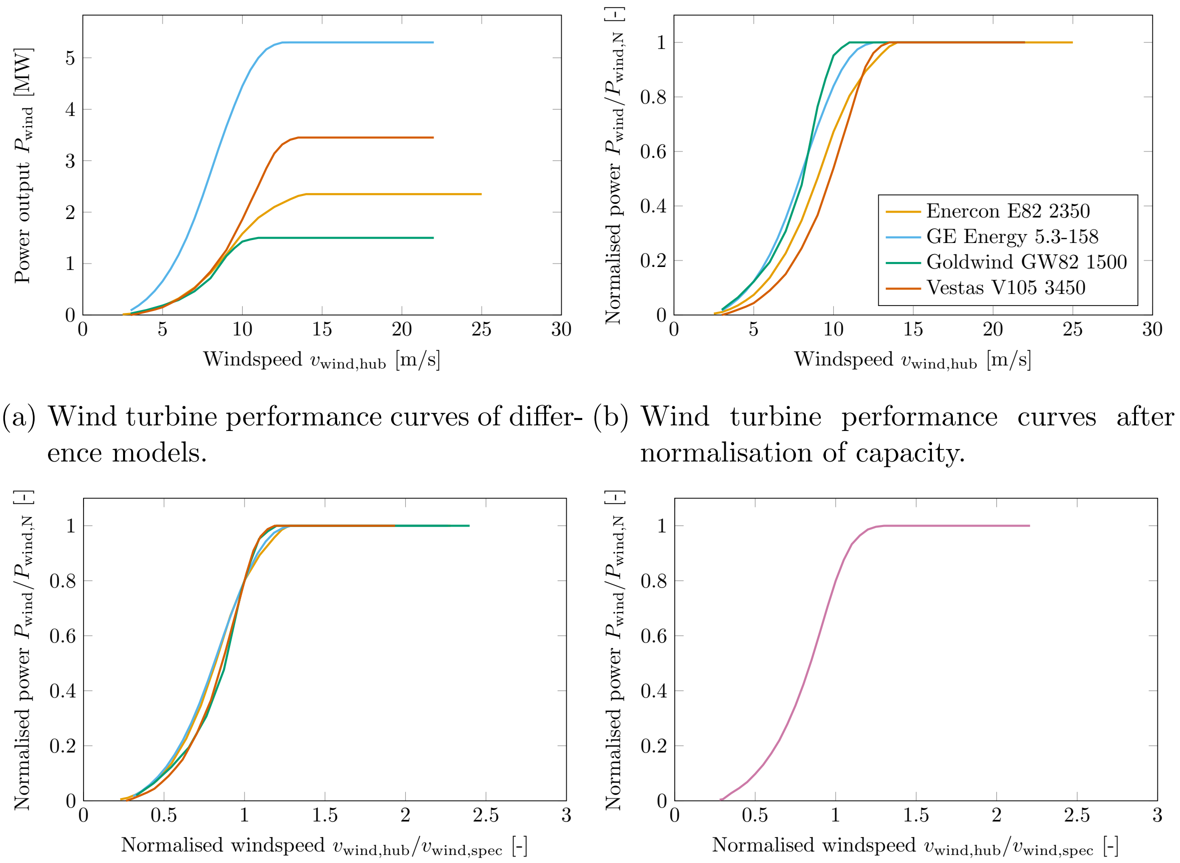

(a) Wind turbine performance curves of difference models.

(b) Wind turbine performance curves after normalisation of capacity.

(c) Wind turbine performance curves after normalisation of capacity and wind speed.

(d) Generic performance curve.

Figure 2.3: Computation of the generic wind turbine performance curve. Original curves taken from [20]. Normalisation of capacity brings the plateau of all curves to the same level. Normalisation of wind speed, using the specific wind speed at which 80 % of the peak capacity is generated, unifies the curves further. The generic curve is the average of all four curves.

turbine cannot harness enough power. For wind speeds above, the breaks in the turbine are applied in order to prevent damages. To compute the generic performance curve, the individual performance curves are normalised and combined. First the curves are normalised by their installed peak capacity $P_{\text{wind,N}}$, see Figure 2.3b. Then the curves are normalised using the specific wind speed $v_{\text{wind,spec}}$ at which the turbine produces 80 % of their peak capacity, see Figure 2.3c. The generic performance curve $\eta_{wind}(-)$ is the average of all normalised curves, see Figure 2.3d. The generated power by a single turbine can now be computed by

$$P_{\text{wind}} = P_{\text{wind,N}} \cdot \eta_{wind} \left(\frac{v_{\text{wind,hub}}}{v_{\text{wind,spec}}} \right). \tag{2.8}$$

Parameter	Value
$v_{\text{wind,spec}}$	$10.205\,\text{m/s}$
$v_{\text{wind,low}}$	$2.875\,\text{m/s}$
$v_{\text{wind,up}}$	$22.75\,\text{m/s}$

Table 2.3: Specific wind speed and cut off wind speeds for the generic performance curve.
All wind speeds are the average values of the four considered performance curves, which are taken from [20].

The specific wind speed and cut off wind speeds are given in Table 2.3.

Normally the wind speed v_{wind} is measured at a given height H_{measure}. To compute the wind speed at hub height $v_{\text{wind,hub}}$, the atmospheric boundary layer

$$v_{\text{wind,hub}} = v_{\text{wind}} \cdot \frac{\ln(H_{\text{hub}}/Z_0)}{\ln(H_{\text{measure}}/Z_0)}, \tag{2.9}$$

is used with Z_0 as the ground roughness, an empirical value based on the composition of the surrounding area.

In order to fully specify the generic turbine used in this model, a hub height of $H_{\text{hub}} = 140\,\text{m}$ and peak capacity of $P_{\text{wind,N}} = 4\,\text{MW}$ are chosen.

The generated power of the wind component can now be computed by

$$P_{\text{wind}} = N_{\text{wind}} \cdot P_{\text{wind,N}} \cdot \eta_{\text{wind}} \left(\frac{v_{\text{wind,hub}}}{v_{\text{wind,spec}}} \right), \tag{2.10}$$

where N_{wind} is the number of installed turbines.

Figure 2.4 gives a schematic representation of the wind component with its inputs and outputs.

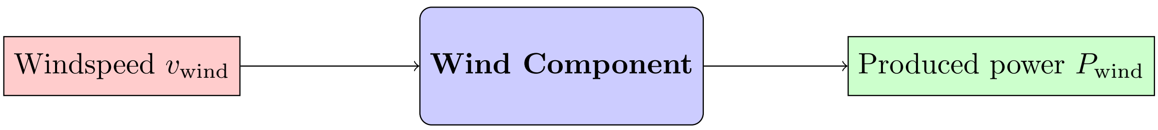

Figure 2.4: Block diagram of the wind component.
The wind speed is a model input and the produced power is a model output of the wind component.

Considering the investment and maintenance costs, Lüers et al. [43] give an overview for costs of onshore wind turbines in Germany, scaled by their installed capacity and hub height. Using the chosen capacity of 4 MW and hub height of 140 m, the total investment costs I_{wind} can be computed by

$$I_{\text{wind}} = N_{\text{wind}} \cdot i_{\text{wind}}. \tag{2.11}$$

Parameter	Value
i_{wind}	4.7 M€
m_{wind}	224 k€/a

Table 2.4: Specific investment and maintenance costs for the wind component. The specific costs are adapted from [43].

The maintenance costs M_{wind} can be computed by

$$M_{\text{wind}} = N_{\text{wind}} \cdot m_{\text{wind}}, \tag{2.12}$$

The specific investment and maintenance costs are listed in Table 2.4.

2.2.3. Biogas Component

Biogas plants use anaerobic digestion to produce biogas from organic matter. The gas can either be injected into the gas grid or turned into thermal and electric energy using an on-site combined heat and power (CHP) system. We focus on electricity generating biogas plants.

Traditionally biogas plants produce electricity at a constant rate, but there are efforts to flexibilise biogas power generation [21]. Modelling a flexible biogas plant is advantageous, due to the fact that the flexible power output of the biogas component can fill possible gaps between demand and supply without using storage components.

In order to develop a flexible model, we take a model for a traditional biogas plant and extend it to allow for flexible power generation. The power output of a traditional biogas plant P_{biogas} is equal to the electric capacity of the CHP system $P_{\text{biogas,N}}$. The annual amount of feedstock consumed by the plant $\dot{m}_{\text{biogas}}$ is constant and can be correlated to the electric capacity:

$$P_{\text{biogas,N}} = \dot{m}_{\text{biogas}} \cdot \frac{109\,000\,\text{m}^3/\text{kt} \cdot 5.97\,\text{kWh}_{\text{ch}}/\text{m}^3 \cdot 0.3\,\text{kWh}_{\text{e}}/\text{kWh}_{\text{ch}}}{8760\,\text{h/a}}. \tag{2.13}$$

The volume of biogas per kilo tonne of feedstock, $109\,000\,\text{m}^3/\text{kt}$, is taken from a survey of United Kingdom based biogas plants [54]. The amount of chemical energy per volume biogas is $5.97\,\text{kWh}_{\text{ch}}/\text{m}^3$ [51]. The electric efficiency of a CHP system is $0.3\,\text{kWh}_{\text{e}}/\text{kWh}_{\text{ch}}$ [51].

McKendry [48] gives an overview of investment and maintenance costs of power generating biogas plants in the United Kingdom. The metric for the investment costs is

$$I_{\text{biogas,base}} = \dot{m}_{\text{biogas}} \cdot 0.1828\,\text{M€ a/kt} + 0.2995\,\text{M€}. \tag{2.14}$$

The metric for the maintenance costs is

$$M_{\mathrm{biogas,base}} = \dot{m}_{\mathrm{biogas}} \cdot 16.669\,\mathrm{k€/kt} + 518.968\,\mathrm{k€/a}, \tag{2.15}$$

and already includes costs for feedstock and disposal of waste.

Both metrics use the annual feedstock capacity as the capacity measure of the biogas plants. Using Equation (2.13), we can express the costs in terms of the electric capacity:

$$I_{\mathrm{biogas,base}} = P_{\mathrm{biogas,N}} \cdot 8.2027\,\mathrm{k€/kW_e} + 299.5\,\mathrm{k€}, \tag{2.16}$$

$$M_{\mathrm{biogas,base}} = P_{\mathrm{biogas,N}} \cdot 0.748\,\mathrm{k€/(kW_e\,a)} + 518.968\,\mathrm{k€/a}. \tag{2.17}$$

The model is flexibilised by adding a gas tank with a storage volume $V_{\mathrm{biogas,N}}$ and an additional CHP system with electric capacity $P_{\mathrm{biogas,N,add}}$.

The generated power is now flexible and is bounded by the electric capacities:

$$0 \leq P_{\mathrm{biogas}} \leq P_{\mathrm{biogas,N}} + P_{\mathrm{biogas,N,add}}. \tag{2.18}$$

We neglect changing part load efficiencies.

The amount of consumed feedstock remains constant, resulting in a constant volume of gas generated $\dot{V}_{\mathrm{biogas,gen}}$. Because the amount of consumed feedstock is determined by the electric capacity of the base CHP system, we can calculate the volume of generated gas from the electric capacity of the base CHP system:

$$\begin{aligned}\dot{V}_{\mathrm{biogas,gen}} &= P_{\mathrm{biogas,N}} \cdot (5.97\,\mathrm{kWh_{ch}/m^3} \cdot 0.3\,\mathrm{kWh_e/kWh_{ch}})^{-1} \\ &= P_{\mathrm{biogas,N}} \cdot 0.558\,\mathrm{m^3/kWh_e},\end{aligned} \tag{2.19}$$

using the inverse of the CHP electric efficiency and chemical energy per volume biogas.

The volume of gas consumed by both CHP systems depends on the power generated:

$$\dot{V}_{\mathrm{biogas,con}} = P_{\mathrm{biogas}} \cdot 0.558\,\mathrm{m^3/kWh_e}, \tag{2.20}$$

using the same correlation between electric energy and volume of biogas.

The volume of gas in the storage tank V_{biogas} is determined by the volume generated and consumed using a state equation:

$$V_{\mathrm{biogas}}(t) = V_{\mathrm{biogas}}(t - \Delta t) + (\dot{V}_{\mathrm{biogas,gen}}(t) - \dot{V}_{\mathrm{biogas,con}}(t)) \cdot \Delta t, \tag{2.21}$$

while not exceeding the capacity of the tank

$$0 \leq V_{\mathrm{biogas}} \leq V_{\mathrm{biogas,N}}. \tag{2.22}$$

[21] provides investment costs for retrofitting existing biogas plants for flexibility. The costs for the tank $I_{\text{biogas,stor}}$ depend on the volume:

$$I_{\text{biogas,stor}} = V_{\text{biogas,N}} \cdot 20.5\,€/\text{m}^3. \tag{2.23}$$

The costs for the additional CHP system $I_{\text{biogas,add}}$ depend on the electric capacity:

$$I_{\text{biogas,add}} = P_{\text{biogas,N,add}} \cdot 858\,€/\text{kW}_\text{e}. \tag{2.24}$$

The total investment costs I_{biogas} is the sum of the costs of the individual components

$$\begin{aligned} I_{\text{biogas}} &= I_{\text{biogas,base}} + I_{\text{biogas,add}} + I_{\text{biogas,stor}} \\ &= P_{\text{biogas,N}} \cdot i_{\text{biogas}} + i_{\text{biogas,const}} \\ &+ P_{\text{biogas,N,add}} \cdot i_{\text{biogas,add}} \\ &+ V_{\text{biogas,N}} \cdot i_{\text{biogas,stor}}. \end{aligned} \tag{2.25}$$

The total maintenance costs M_{biogas} only consist of the maintenance costs of the main biogas plant

$$M_{\text{biogas}} = M_{\text{biogas,base}} = P_{\text{biogas,N}} \cdot m_{\text{biogas}} + m_{\text{biogas,const}}. \tag{2.26}$$

The specific investment and maintenance costs are listed in Table 2.5.

Figure 2.5 gives a schematic representation of the biogas component with its inputs and outputs.

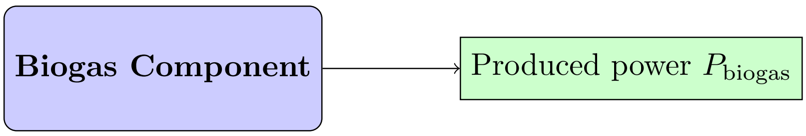

Figure 2.5: Block diagram of the biogas component.
The produced power is a model output of the biogas component.

Parameter	Value
i_{biogas}	$8.2027\,\text{k}€/\text{kW}_\text{e}$
$i_{\text{biogas,const}}$	$299.5\,\text{k}€$
$i_{\text{biogas,add}}$	$858\,€/\text{kW}_\text{e}$
$i_{\text{biogas,stor}}$	$20.5\,€/\text{m}^3$
m_{biogas}	$0.748\,\text{k}€/(\text{kW}_\text{e}\,\text{a})$
$m_{\text{biogas,const}}$	$518.968\,\text{k}€/\text{a}$

Table 2.5: Specific investment and maintenance costs for the biogas component.
The calculations for the specific costs are detailed in Equations (2.13) to (2.17), Equation (2.23) and Equation (2.24).

2.2.4. Hydroelectric Component

Hydroelectricity produces electric power from the flow of water by letting the water flow through a set of turbines. Because hydroelectricity can produce electricity at a more stable, reliable and cheaper rate than other renewable energy sources, hydroelectricity is an established form of renewable energy [30]. Additionally, hydroelectricity exhibits a high dependence on local factors like the existence of a running body of water and suitable construction site for turbines and dams, limiting the number of potential construction sites. This makes it less favourable for optimisation because many of the limited number of construction sites are already occupied by existing plants. However, the comparatively low cost of electricity makes hydroelectricity essential for a transition to renewable energy. So it should be considered when designing a DES for a city.

There are two main types of hydroelectric plants. Conventional plants, which use a dam to create a more energetic flow of water by raising the height difference between the water levels before and after the turbine, and run-of-the-river (ROR) plants, which only use the natural flow of a river. Conventional plants have advantages over ROR plants. They can control the amount of water that is flowing through the turbines, and therefore the amount of generated power, while ROR plants are subject to fluctuating flow rates. Disadvantages of conventional plants are higher costs of installation and a more limited number of available sites. In this work, we focus on ROR plants, because possible sites for ROR plants are more numerous than for conventional dams.

We assume constant flow of water and therefore a constant power output P_{hydro} equal to the electric capacity $P_{\text{hydro,N}}$ of the turbines installed in the plant:

$$P_{\text{hydro}} = P_{\text{hydro,N}}. \tag{2.27}$$

Figure 2.6 gives a schematic representation of the hydroelectric component with its inputs and outputs.

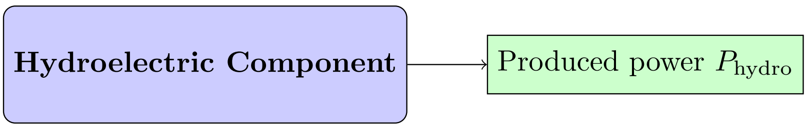

Figure 2.6: Block diagram of the hydroelectric component.
The produced power is a model output of the hydroelectric component.

Hofer [30] analyses the investment and maintenance costs of a large number of ROR plants all over Europe. The total investment costs I_{hydro} are scaled using the installed capacity:

$$I_{\text{hydro}} = P_{\text{hydro,N}} \cdot i_{\text{hydro}}. \tag{2.28}$$

The maintenance costs M_{hydro} are a set as a fraction of the investment costs and can therefore be expressed in terms of installed capacity:

$$M_{\text{hydro}} = 0.16/\text{a} \cdot I_{\text{hydro}} = P_{\text{hydro,N}} \cdot m_{\text{hydro}}. \tag{2.29}$$

Parameter	Value	Source
i_{hydro}	3200 €/kW	[30]
m_{hydro}	512 €/(kW a)	[a]

Table 2.6: Specific investment and maintenance costs for the hydroelectric component.
[a] The maintenance cost are 16 % of the investment costs [30].

The specific investment and maintenance costs are listed in Table 2.6.

2.3. Storage Systems

Storage systems are essential for designing a self-sufficient energy system using renewable power plants. They convert excessive electric energy into forms of energy that can be easily stored and later turned back into electric energy if the power plants are not able to meet the demands.

In this work, we focus on four different technologies: pumped hydropower, hydrogen storage, Power-to-Gas (PtG), and battery storage. The models for all technologies are similar, so we present it for a generic technology l before discussing each technology and their specific parameters.

The storage component consists of a charging unit, a storage unit and a discharging unit.

The power charged into the storage unit $P_{\text{l,char}}$ is bounded by the capacity of the charging unit $P_{\text{l,char,N}}$

$$0 \leq P_{\text{l,char}} \leq P_{\text{l,char,N}}. \tag{2.30}$$

The power discharged from the storage unit $P_{\text{l,dis}}$ is bounded by the capacity of the discharging unit $P_{\text{l,dis,N}}$

$$0 \leq P_{\text{l,dis}} \leq P_{\text{l,dis,N}}. \tag{2.31}$$

The amount of energy stored Q_{l} must change according to the charging and discharging rates, following a state equation:

$$Q_{\text{l}}(t) = Q_{\text{l}}(t - \Delta t) + (P_{\text{l,char}}(t) \cdot \eta_{\text{l,char}} - P_{\text{l,dis}}(t) \cdot \eta_{\text{l,dis}}^{-1}) \cdot \Delta t - Q_{\text{l}}(t - \Delta t) \cdot \eta_{\text{l,self}}, \tag{2.32}$$

were $\eta_{\text{l,char}}$ is the charging efficiency, $\eta_{\text{l,dis}}$ the discharging efficiency and $\eta_{\text{l,self}}$ the self-discharging rate. These factors depend on the technology and are derived below. Parasitic energy consumption used to operate the charging and discharging units are incorporated into the conversion losses.

The amount of stored energy must not exceed the storage capacity $Q_{\text{l,N}}$

$$0 \leq Q_{\text{l}} \leq Q_{\text{l,N}}. \tag{2.33}$$

Figure 2.7 gives a schematic representation of a generic storage component with its inputs and outputs.

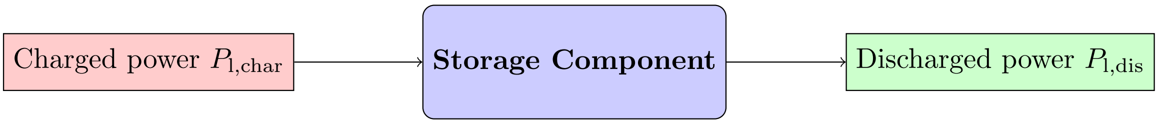

Figure 2.7: Block diagram of a generic storage component.
The charged power is a model input and the discharged power is a model output of a generic storage component.

The total investment costs I_{l} consist of the costs for the charging, discharging and storage units

$$I_{\mathrm{l}} = P_{\mathrm{l,char,N}} \cdot i_{\mathrm{l,char}} + P_{\mathrm{l,dis,N}} \cdot i_{\mathrm{l,dis}} + Q_{\mathrm{l,N}} \cdot i_{\mathrm{l,stor}}, \tag{2.34}$$

where $i_{\mathrm{l,char}}$, $i_{\mathrm{l,dis}}$ and $i_{\mathrm{l,stor}}$ are the specific investment costs of the charging, discharging and storage units. These factors depend on the technology and are derived below.

Analogous to the investment costs, total maintenance costs M_{l} are computed from the installed capacities

$$M_{\mathrm{l}} = P_{\mathrm{l,char,N}} \cdot m_{\mathrm{l,char}} + P_{\mathrm{l,dis,N}} \cdot m_{\mathrm{l,dis}} + Q_{\mathrm{l,N}} \cdot m_{\mathrm{l,stor}}, \tag{2.35}$$

using specific costs $m_{\mathrm{l,char}}$, $m_{\mathrm{l,dis}}$ and $m_{\mathrm{l,stor}}$ that are technology dependent.

2.3.1. Pumped Hydropower

Pumped hydropower stores energy by pumping water from a lower reservoir into a higher reservoir, converting electric energy into potential energy. Later, the water can flow from the higher into the lower reservoir spinning turbines that generate electric power. Similar to hydroelectricity pumped hydropower is limited by suitable sites. If a suitable site is available, pumped hydropower can offer large storage capacities.

Usually, the capacity is measured in m^3 of movable water. Together with the height difference between the reservoirs, the storage capacity can be expressed in kWh of stored potential energy. As the literature presents costs in terms of potential energy, we quantify the storage capacity in kWh.

Hartmann et al. [28] give an overview on efficiencies, see Table 2.7. Self-discharging through water evaporation in the upper reservoir is neglected. Conrad et al. [16] give an overview of the investment and maintenance costs. The investment costs I_{pump} based on the installed capacities can be expressed as

$$\begin{aligned} I_{\mathrm{pump}} = {} & P_{\mathrm{pump,char,N}} \cdot i_{\mathrm{pump,char}} \\ & + P_{\mathrm{pump,dis,N}} \cdot i_{\mathrm{pump,dis}} \\ & + Q_{\mathrm{pump,N}} \cdot i_{\mathrm{pump,stor}}, \end{aligned} \tag{2.36}$$

where the combined costs for the charging and discharging units are equally split. The maintenance costs M_{pump} are split into fixed and variable costs. The fixed costs, combined for the charging and discharging units, are equally split. The variable costs are scaled using the number of pump and turbine starts per year, $N_{\text{start,pump}}$, $N_{\text{start,tur}}$ and total generated power per year Q_{total}

$$
\begin{aligned}
M_{\text{pump}} = {} & N_{\text{start,pump}} \cdot P_{\text{pump,char,N}} \cdot 8.95\,€/\text{MW} \\
& + N_{\text{start,tur}} \cdot P_{\text{pump,dis,N}} \cdot 3.34\,€/\text{MW} \\
& + Q_{\text{total}} \cdot 0.56\,€/(\text{MW h}) \\
& + P_{\text{pump,char,N}} \cdot 1.43\,€/(\text{kW a}) \\
& + P_{\text{pump,dis,N}} \cdot 1.43\,€/(\text{kW a}).
\end{aligned}
\tag{2.37}
$$

Most pumped hydropower plants in Germany are designed as daily storages, executing a daily charging and discharging cycle [28]. Assuming that the storage performs one cycle per day, discharging 75 % of its storage capacity, we can express the maintenance costs in terms of installed capacity as

$$
\begin{aligned}
M_{\text{pump}} = {} & 365/\text{a} \cdot P_{\text{pump,char,N}} \cdot 8.95\,€/\text{MW} \\
& + 365/\text{a} \cdot P_{\text{pump,dis,N}} \cdot 3.34\,€/\text{MW} \\
& + 0.75 \cdot 0.91 \cdot 365/\text{a} \cdot Q_{\text{pump,N}} \cdot 0.56\,€/\text{MWh} \\
& + P_{\text{pump,char,N}} \cdot 1.43\,€/(\text{kW a}) \\
& + P_{\text{pump,dis,N}} \cdot 1.43\,€/(\text{kW a}) \\
= {} & P_{\text{pump,char,N}} \cdot m_{\text{pump,char}} \\
& + P_{\text{pump,dis,N}} \cdot m_{\text{pump,dis}} \\
& + Q_{\text{pump,N}} \cdot m_{\text{pump,stor}},
\end{aligned}
\tag{2.38}
$$

where we incorporate the discharging efficiency of 0.91 into the computation of Q_{total}. Table 2.7 provides all calculated values for the pumped hydropower component.

Parameter	Value	Source
$i_{\text{pump,char}}$	529.62 €/kW	
$i_{\text{pump,dis}}$	529.62 €/kW	
$i_{\text{pump,stor}}$	1.3 €/kWh	
$m_{\text{pump,char}}$	4.696 75 €/(kW a)	
$m_{\text{pump,dis}}$	2.6491 €/(kW a)	
$m_{\text{pump,stor}}$	0.139 503 €/(kWh a)	
$\eta_{\text{pump,char}}$	0.88	[28]
$\eta_{\text{pump,dis}}$	0.91	[28]
$\eta_{\text{pump,self}}$	0	[a]

Table 2.7: Specific investment and maintenance costs and technical parameters for pumped hydropower.
The calculations for the specific costs are detailed in Equations (2.36) to (2.38). [a] Neglected

Parameter	Alkaline	PEM	SOEC
$i_{\mathrm{h,char}}$	925 €/kW [a]	2090 €/kW [a]	6000 €/kW [b]
$i_{\mathrm{h,dis}}$	3000 €/kW [b]	2090 €/kW [a]	6000 €/kW [b]
$m_{\mathrm{h,char}}$	18.5 €/(kW a) [c]	41.8 €/(kW a) [c]	120 €/(kW a) [c]
$m_{\mathrm{h,dis}}$	60 €/(kW a) [c]	41.8 €/(kW a) [c]	120 €/(kW a) [c]
$\eta_{\mathrm{h,char}}$	0.71 [b]	0.63 [b]	0.82 [b]
$\eta_{\mathrm{h,dis}}$	0.60 [b]	0.56 [b]	0.50 [b]

Table 2.8: Specific investment and maintenance costs and technical parameters for electrolysis and fuel cells.
[a] [3], [b] [22], [c] The maintenance costs are 2 % of the investment costs, as suggested by [3].

2.3.2. Hydrogen Storage

Hydrogen storages use excess electric energy to split water into hydrogen and oxygen using an electrolyser. The hydrogen can be stored and combined with oxygen back into water inside a fuel cell, providing electric energy.

The Fuel Cells and Hydrogen Joint Undertaking [3] and Ferrero et al. [22] both investigate the potential of hydrogen storage. Three different hydrogen electrolysis and fuel cell technologies where considered: Alkaline, Proton exchange Membrane (PEM) and Solid Oxide Electrolysis cells (SOEC). Table 2.8 provides the specific investment and maintenance costs together with the electric efficiencies for the charging and discharging units.

The generated hydrogen has to be stored. Underground caverns provide large volumes for storage. Suitable caverns are however only available at certain locations, and hydrogen competes with oil, natural gas and heating as possible storage applications for caves. An alternative are on-site high pressure steel tanks, which are currently used for small-scale storages.

We focus on on-site high pressure steel tanks, as there is no need for hydrogen transport to a possibly far away cavern. The operation of high-pressure steel tanks needs compressors. The installation costs are already factored into the specific investment costs of the steel tanks [4]. Any parasitic energy needs are already factored into the efficiencies of the fuel cells [22].

Table 2.9 provides the specific investment and maintenance costs for the storage units. Gas leakage from the tanks is neglected, leading to no self-discharging.

Parameter	Value
$i_{\mathrm{h,stor}}$	20 €/kWh [a]
$m_{\mathrm{h,stor}}$	0.4 €/(kWh a) [b]
$\eta_{\mathrm{h,self}}$	0 [c]

Table 2.9: Specific investment and maintenance costs and technical parameters for hydrogen storage.
[a] [4], [b] The maintenance costs are 2 % of the investment costs., [c] Neglected

Parameter	Chemical	Biological	Source
$i_{\text{ch4,char}}$	2211.84 €/kW	2315.52 €/kW	[57]
$i_{\text{ch4,dis}}$	858 €/kW	858 €/kW	[21]
$m_{\text{ch4,char}}$	78.795 €/(kW a)	72.095 €/(kW a)	[57]
$m_{\text{ch4,dis}}$	0 €/(kW a)	0 €/(kW a)	[21]
$\eta_{\text{ch4,char}}$	0.568	0.568	[57]
$\eta_{\text{ch4,dis}}$	0.3	0.3	[51]

Table 2.10: Specific investment and maintenance costs and technical parameters for methanisation and CHP systems.

2.3.3. Power-to-Gas

Power-to-Gas (PtG) generates methane gas from electricity using a two step process. First, electrolysis provides hydrogen. In the second step, the hydrogen is reacted with carbon dioxide to form methane, also called synthetic natural gas. The produced methane can be put to different uses. Fuelling vehicles, injecting it into the natural-gas grid, or burning it to generate heat and electricity. We focus on storing the methane on site and converting it back into electric energy using a gas turbine.

Van Leeuwen and Zauner [57] provide the investment, maintenance and feedstock costs as well as efficiencies of PtG plants for two technologies, namely chemical and biological methanisation. The PtG plant investigated by Van Leeuwen and Zauner injects the generated gas into the gas grid. The costs for the gas grid injection station are disregarded as we store the methane on site.

Feedstock for PtG include water and carbon dioxide. The costs for water are disregarded. Carbon dioxide is captured from the exhaust gases from burning the methane, leading to a closed carbon cycle. The costs of the carbon capturing and storage facilities are neglected.

As the generated methane is similar to the gas generated by a biogas plant, the same storage tanks and gas turbines can be used. The specific investment and maintenance costs of the storage tanks in the biogas component, see Table 2.5, are given per volume of biogas. Multiplying the specific costs with the amount of chemical energy per volume biogas, $5.97\,\text{kWh}_{\text{ch}}/\text{m}^3$ [51], the specific investment and maintenance costs of the methane storage can be given per amount of stored energy

$$i_{\text{ch4,stor}} = i_{\text{biogas,stor}} \cdot 5.97\,\text{kWh}_{\text{ch}}/\text{m}^3 \tag{2.39}$$

$$m_{\text{ch4,stor}} = m_{\text{biogas,stor}} \cdot 5.97\,\text{kWh}_{\text{ch}}/\text{m}^3 \tag{2.40}$$

Table 2.10 provides the costs and efficiencies for both methanisation technologies and CHP systems. Table 2.11 provides the costs and efficiencies for the methane storage tank.

Parameter	Value	Source
$i_{\text{ch4,stor}}$	3.444 €/kWh	
$m_{\text{ch4,stor}}$	0 €/(kWh a)	
$\eta_{\text{ch4,self}}$	0	[a]

Table 2.11: Specific investment and maintenance costs and technical parameters for methane storage.
The calculations for the specific costs are detailed in Equations (2.39) and (2.40). [a] Neglected

2.3.4. Battery Storage

Batteries use electro chemical processes to store electric energy, offering up high round trip efficiencies.

A constraint of battery storage is that batteries have a maximum depth of discharge $q_{\text{bat,max}}$. We incorporate it into the component model by replacing the lower bound of Equation (2.33) with $(1 - q_{\text{bat,max}}) \cdot Q_{\text{bat,N}}$.

Jülch et al. [32] give an overview of costs and efficiencies of three different battery storage technologies: Lithium-ion (Li-Ion), Lead (Pb) and Vanadium-Redox-Flow (VRF). Only round trip efficiencies are provided so the losses are evenly split between charging and discharging efficiencies. Table 2.12 provides the costs, efficiencies and maximum depth of discharge for all three technologies.

Parameter	Li-ion	Pb	VRF
$i_{\text{bat,char}}$	0 €/kW	0 €/kW	0 €/kW
$i_{\text{bat,dis}}$	80 €/kW	80 €/kW	0 €/kW
$i_{\text{bat,stor}}$	855 €/kWh	280 €/kWh	985 €/kWh
$m_{\text{bat,char}}$	0 €/(kW a) [a]	0 €/(kW a) [a]	0 €/(kW a) [a]
$m_{\text{bat,dis}}$	1.6 €/(kW a) [a]	1.6 €/(kW a) [a]	0 €/(kW a) [a]
$m_{\text{bat,stor}}$	17.1 €/(kWh a) [a]	5.6 €/(kWh a) [a]	19.7 €/(kWh a) [a]
$\eta_{\text{bat,char}}$	0.975	0.877	0.894
$\eta_{\text{bat,dis}}$	0.975	0.877	0.894
$\eta_{\text{bat,self}}$	0.01 per Month	0.02 per Month	0.0083 per Month
$q_{\text{bat,max}}$	0.8	0.5	1

Table 2.12: Specific investment and maintenance costs and technical parameters for battery storage [32].
[a] The maintenance costs are 2 % of the investment costs [32].

2.4. Consumption Component

The consumption component represents the city that the DES tries to supply with electricity. The energy demand P_{demand} is given as a time series of parameters. Figure 2.8 gives a schematic representation of a consumption component with its inputs and outputs.

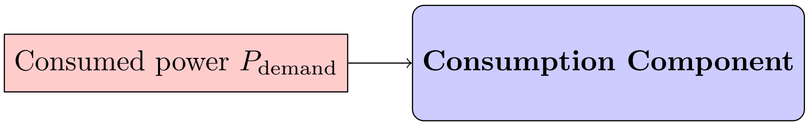

Figure 2.8: Block diagram of the consumption component.
The consumed power is a model input of the consumption component.

2.5. Grid Component

A connection of the DES to the national electricity grid is represented using the grid component. If not enough energy is available in the local energy grid, the discrepancy can be purchased from the grid P_{buy}, generating costs. Excess energy can be sold, P_{sell}, generating revenue, here modelled as negative costs.

This work focuses on optimal DES design, so we do not consider regulations when connecting to energy markets. These problems can be tackled by bidding strategies and virtual power plants in energy markets.

Figure 2.9 gives a schematic representation of a consumption component with its inputs, outputs and variables.

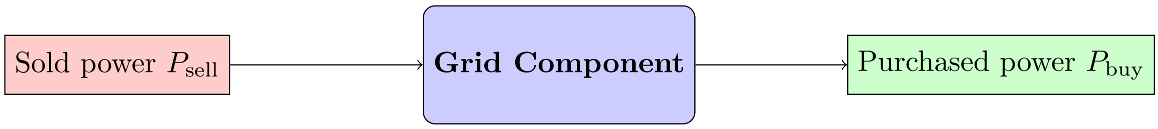

Figure 2.9: Block diagram of the grid component.
The sold power is a model input and the purchased power is a model output of the grid component.

The generated costs C_{grid} are calculated using the electricity tariff c_{buy} and feed-in tariff c_{sell}

$$C_{\text{grid}} = P_{\text{buy}} \cdot c_{\text{buy}} \cdot \Delta t - P_{\text{sell}} \cdot c_{\text{sell}} \cdot \Delta t. \tag{2.41}$$

2.6. Superstructure

In the superstructure, the components are connected to form the DES, which is shown in Figure 2.1 The produced energy consists of the outputs of all power plant components $k \in K$, storage components $l \in L$, and purchased energy from the grid. The electricity is consumed by the storage components, the city or is sold to the grid. Both produced energy and consumed energy must equal at all times

$$\sum_{k \in K} P_{\text{k}} + \sum_{l \in L} P_{\text{l,dis}} + P_{\text{buy}} = \sum_{l \in L} P_{\text{l,char}} + P_{\text{demand}} + P_{\text{sell}}. \tag{2.42}$$

We do not consider distances, losses and maximum load capacities within the local transmission infrastructure.

3. Optimisation under Certainty

In this section, the DES model from Section 2 is embedded into a mixed integer linear program (MILP) for optimal DES design.

A mixed integer linear program is a variant of a linear program (LP). A linear program takes the form

$$\begin{aligned} &\min_x \; c^T x \\ &\text{s.t. } Ax \geq b, \end{aligned} \tag{3.1}$$

where $x \in \mathbb{R}^d$ is a vector of decision variables, $c^T x$ is the linear objective function and $Ax \geq b$ is a set of linear constraints [42]. A set of values for the variables that satisfy all constraints is called a feasible solution. An optimal solution is a solution with the minimum objective value compared to all other feasible solutions.

A given LP can be solved using a host of solvers, each guaranteeing to find a global optimal solution. A LP can be infeasible if no solution exists, or unbounded if the constraints allow for solutions with arbitrary minimal objective values. Solvers can detect if a LP is infeasible or unbounded.

If one or more of the decision variables are restricted to integer values the program is called a MILP. In this case, the complexity of the solving process increases, due to combinatorial complexity. Techniques like branch and bound can be applied to find optimal solutions for MILPs. Sometimes the introduction of integer variables can render a feasible LP infeasible, because there exists no integer solution. The higher the number of integer variables, the higher the chance of infeasibility.

In the context of optimal DES design, the decision variables represent design and operational choices, i.e., equipment sizing or energy flow decisions. The constraints capture the operational behaviour of the DES as well as design limitations, like maximum available land area for solar farms. Additional design goals, like self-sufficiency can be enforced by adding additional constraints to the MILP.

The objective function determines what feature of a DES design should be optimised. In this work, we focus on cost optimal DES design, so the objective function should measure the economic performance of a given DES design.

In this section, first all restrictions of the DES model from Section 2 are translated into linear constraints in Section 3.1. The objective function is developed in Section 3.2, and additional constraints in Section 3.3.

3.1. Model Translation

The descriptions of the DES model from Section 2 are translated into linear constraints.

To capture the operation of the DES, a time series formulation is chosen. All parameters and variables that change over time are given as a series of values with index $t \in T$ for a time series T. The points in the time series are equidistant with a period of Δt. The exact value determines the coarseness of the model and is application dependent. Each constraint that contains a parameter dependent on t must hold for all time steps t in the time series T.

Photovoltaic Component The power generated by the photovoltaic component $P_{\text{pv},t}$ is restricted by

$$0 \leq P_{\text{pv},t} \leq (P_{\text{pv,N,roof}} + P_{\text{pv,N,farm}}) \cdot p_{\text{pv},t} \tag{3.2}$$

with the installed peak capacities on roofs $P_{\text{pv,N,roof}}$ and in solar farms $P_{\text{pv,N,farm}}$ as decision variables. The specific capacity $p_{\text{pv},t}$ is precomputed from the total solar irradiation $G_{\text{T},t}$ and ambient temperature $T_{\text{a},t}$

$$p_{\text{pv},t} = \left(1 - \beta_{\text{ref}} \cdot \left(T_{\text{a},t} - T_{\text{ref}} + (T_{\text{NOCT}} - T_{\text{a},t}) \cdot \frac{G_{\text{T},t}}{G_{\text{NOCT}}}\right)\right) \cdot \frac{G_{\text{T},t}}{G_{\text{ref}}} \tag{3.3}$$

The inequality in Equation (3.2) allows for curtailment of the photovoltaic component. This is necessary to prevent infeasibility in scenarios with full self-sufficiency, see Section 3.3.2.

Wind Component The power generated by the wind component $P_{\text{wind},t}$ is restricted by

$$0 \leq P_{\text{wind},t} \leq N_{\text{wind}} \cdot p_{\text{wind},t}. \tag{3.4}$$

with the installed number of wind turbines N_{wind} as an integer decision variable. The power produced by a single wind turbine $p_{\text{wind},t}$ is precomputed from the measured wind speed $v_{\text{wind},t}$

$$p_{\text{wind},t} = 4\,\text{MW} \cdot \eta_{\text{wind}} \left(\frac{v_{\text{wind,hub},t}}{v_{\text{wind,spec}}}\right). \tag{3.5}$$

$$v_{\text{wind,hub,t}} = v_{\text{wind},t} \cdot \frac{\ln(140\,\text{m}/Z_0)}{\ln(H_{\text{measure}}/Z_0)}. \tag{3.6}$$

Similar to the photovoltaic component, curtailment of the wind component is enabled by turning Equation (3.4) into an inequality. This can prevent infeasibilities in scenarios with full self-sufficiency, see Section 3.3.2.

Biogas Component For the biogas component, the installed CHP base capacity $P_{\text{biogas,N}}$, additional CHP capacity $P_{\text{biogas,N,add}}$ and storage volume $V_{\text{biogas,N}}$ are decision variables. The generated electricity $P_{\text{biogas},t}$ can be chosen within the capacity limits

$$0 \leq P_{\text{biogas},t} \leq P_{\text{biogas,N}} + P_{\text{biogas,N,add}}. \tag{3.7}$$

The stored volume of biogas $V_{\mathrm{biogas},t}$ then follows the discretised state equation

$$V_{\mathrm{biogas},t} = V_{\mathrm{biogas},t-1} + (P_{\mathrm{biogas,N}} \cdot 0.558\,\mathrm{m}^3/\mathrm{kWh_e} - P_{\mathrm{biogas},t} \cdot 0.558\,\mathrm{m}^3/\mathrm{kWh_e}) \cdot \Delta t, \quad (3.8)$$

and must not exceed the storage volume

$$0 \leq V_{\mathrm{biogas},t} \leq V_{\mathrm{biogas,N}}. \quad (3.9)$$

See Section 3.3.3 for additional constraints concerning components with storages.

Hydroelectric Component For the hydroelectric component, the generated energy $P_{\mathrm{hydro},t}$ is equal to the installed capacity $P_{\mathrm{hydro,N}}$ given as a decision variable:

$$P_{\mathrm{hydro},t} = P_{\mathrm{hydro,N}} \quad (3.10)$$

Storage Components Each energy storage component follows the same equations, so we formulate a set of constraints for a generic storage component $l \in L$. The capacity of the charging unit $P_{\mathrm{l,char,N}}$, discharging unit $P_{\mathrm{l,dis,N}}$, and storage unit $Q_{\mathrm{l,N}}$ are decision variables. The power consumed by charging $P_{\mathrm{l,char},t}$ can be chosen within the capacity limits

$$0 \leq P_{\mathrm{l,char},t} \leq P_{\mathrm{l,char,N}}. \quad (3.11)$$

The power generated by discharging $P_{\mathrm{l,dis},t}$ can also be chosen within the capacity limits

$$0 \leq P_{\mathrm{l,dis},t} \leq P_{\mathrm{l,dis,N}}. \quad (3.12)$$

The storage fill level $Q_{\mathrm{l},t}$ follows the discretised state equation

$$Q_{\mathrm{l},t} = Q_{\mathrm{l},t-1} + (P_{\mathrm{l,char},t} \cdot \eta_{\mathrm{l,char}} - P_{\mathrm{l,dis},t} \cdot \eta_{\mathrm{l,dis}}^{-1}) \cdot \Delta t - Q_{\mathrm{l},t-1} \cdot \eta_{\mathrm{l,self}} \quad (3.13)$$

not exceeding the storage capacity and maximum depth of discharge $q_{\mathrm{l,max}}$

$$(1 - q_{\mathrm{l,max}}) \cdot Q_{\mathrm{l,N}} \leq Q_{\mathrm{l},t} \leq Q_{\mathrm{l,N}}. \quad (3.14)$$

See Section 3.3.3 for additional constraints concerning components with storages.

Consumption Component The energy demand of the city $P_{\mathrm{demand},t}$ is provided as time series of parameters.

Grid Component The amount of purchased energy $P_{\mathrm{buy},t}$ and sold energy $P_{\mathrm{sell},t}$ are decision variables.

Superstructure The energy balance of the local electricity grid is

$$\sum_{k \in K} P_{\mathrm{k},t} + \sum_{l \in L} P_{\mathrm{l,dis},t} + P_{\mathrm{buy},t} = \sum_{l \in L} P_{\mathrm{l,char},t} + P_{\mathrm{demand},t} + P_{\mathrm{sell},t}. \tag{3.15}$$

3.2. Objective Function

In the context of designing an optimal DES, the objective function defines the features of a given DES design that are of interest. Usually, these cover the cost of installing and operating the DES. Sometimes other features could also be included, like environmental impact or certain energy shares. In this work, we focus on optimising the cost of a DES, while guaranteeing a high degree of self-sufficiency using additional constraints, see Section 3.3.

The cost of a DES can usually be split into two categories. The upfront investment costs, to be paid before the DES is operational, and maintenance costs, paid during the operation of the DES. Investment costs typically include planning, permissions, land, materials, construction and margins for foreseeable spare parts. Maintenance costs include personnel costs, leasing, insurance, repairs and replacements. They are typically given as annual costs. Depending on the source, costs for fuel and waste disposal are included in the maintenance costs or treated separately. In our case, they are included in the maintenance costs. The computation of total investment costs and yearly maintenance costs for each power generating and energy storage component are detailed in Section 2. Additionally, the DES can buy and sell energy from the external grid, further generating costs, or revenue

$$C_{\mathrm{grid}} = \sum_{t \in T} P_{\mathrm{buy},t} \cdot c_{\mathrm{buy}} \cdot \Delta t - P_{\mathrm{sell},t} \cdot c_{\mathrm{sell}} \cdot \Delta t. \tag{3.16}$$

where c_{buy} is the electricity price for purchasing electricity from the external grid and c_{sell} the feed-in tariff for selling electricity to the grid.

When regarding the true cost of a DES, one has to take into account its life time. Either by computing maintenance costs over the whole lifetime from the yearly costs, or by spreading the one-time investment costs over the economic lifetime. Usually the second approach, called annualisation, is performed. For a given producing or storing component $i \in K \cup L$ the investment costs I_{i} are annualised using the annuity present value factor $APVF_{\mathrm{i}}$ [36]

$$APVF_{\mathrm{i}} = \frac{r \cdot (1+r)^{a_i}}{(1+r)^{a_i} - 1} \quad \forall i \in K \cup L, \tag{3.17}$$

where a_i is the economic lifetime of component i in years and r the interest rate, usually set to 0.05. The economic lifetime of all components are listed in Table 3.1.

Component	Economic Lifetime	Source
Photovoltaic	25 a	[36]
Wind	25 a	[36]
Biogas	30 a	[36]
Hydroelectric	80 a	[a]
Pumped Hydropower	80 a	[32]
Hydrogen	20 a	[22]
Power-to-Gas	20 a	[57]
Li-ion [b]	20 a [c]	[32]
Pb [b]	10 a [c]	[32]
VRF [b]	20 a [c]	[32]

Table 3.1: Economic lifetime of power producing and energy storage components.
[a] Similar to pumped hydropower, [b] Lifetime of battery storage depends on technology used, [c] Based on daily charging cycles [32]

The annualised investment costs I of the DES is the sum of the individual annualised investment costs

$$I = \sum_{i \in K \cup L} I_{\mathrm{i}} \cdot APVF_{\mathrm{i}}. \tag{3.18}$$

The maintenance costs M is the sum of the individual maintenance costs

$$M = \sum_{i \in K \cup L} M_{\mathrm{i}}. \tag{3.19}$$

The grid component is the only component that contributes to the additional costs

$$C = n_{\mathrm{period}} \cdot C_{\mathrm{grid}}. \tag{3.20}$$

where the factor n_{period} is used to adjust the time covered the time series T to the length of a year.

The final objective function is the total annual costs TAC

$$TAC = I + M + C. \tag{3.21}$$

3.3. Additional Constraints

Additional constraints can be used to enforce special design goals and limitations into the optimisation problem.

3.3.1. Capacity Limits

The main design limitations of DES designs are limitations on component sizes. This is enforced by providing a maximal allowed capacity for each decision variable that represents the capacity of a component

$$P_{\text{pv,N,roof}} \leq P^{\text{max}}_{\text{pv,N,roof}} \tag{3.22}$$
$$P_{\text{pv,N,farm}} \leq P^{\text{max}}_{\text{pv,N,farm}} \tag{3.23}$$
$$N_{\text{wind}} \leq N^{\text{max}}_{\text{wind}} \tag{3.24}$$
$$P_{\text{biogas,N}} \leq P^{\text{max}}_{\text{biogas,N}} \tag{3.25}$$
$$P_{\text{biogas,N,add}} \leq P^{\text{max}}_{\text{biogas,N,add}} \tag{3.26}$$
$$V_{\text{biogas,N}} \leq V^{\text{max}}_{\text{biogas,N}} \tag{3.27}$$
$$P_{\text{hydro,N}} \leq P^{\text{max}}_{\text{hydro,N}} \tag{3.28}$$
$$P_{\text{l,char,N}} \leq P^{\text{max}}_{\text{l,char,N}} \quad \forall l \in L \tag{3.29}$$
$$P_{\text{l,dis,N}} \leq P^{\text{max}}_{\text{l,dis,N}} \quad \forall l \in L \tag{3.30}$$
$$Q_{\text{l,N}} \leq Q^{\text{max}}_{\text{l,N}} \quad \forall l \in L. \tag{3.31}$$

3.3.2. Self-sufficiency

The design goal of self-sufficiency can be expressed using additional constraints. We express two different kinds of self-sufficiency, namely full and partial self-sufficiency.

Full self-sufficiency A DES is fully self-sufficient if the connection to the external grid is not utilised. This could be realised by removing the grid component or setting the variables for purchased and sold energy to zero. Such a formulation can result in infeasible problems. Consider a scenario containing an extreme period of low supply and peak demand, as well as an extreme period of peak supply and low demand. In the worst case, no DES design within the given design constraints can function during both extreme periods. Either energy has to be purchased during the low supply, peak demand period or energy has to be sold during the peak supply, low demand period.

In order to circumvent such infeasibilities we employ an alternative strategy to enforce full self-sufficiency. The variables for purchased energy are set to zero, forcing the DES to produce enough energy to bridge the low supply, peak demand periods. This could lead to overproduction during the peak supply, low demand period. The DES can compensate the overproduction by emptying its storages or curtailing its production components. We emulate the emptying and curtailment by setting the feed in energy tariff c_{sell} to zero. This enables the DES to get rid of energy without incentivising it by earning revenue. Additionally, direct curtailment is built into the solar and wind components by using inequalities in Equations (3.2) and (3.4).

Partial self-sufficiency Partial self-sufficiency allows a fraction of the consumed energy to be purchased from the grid, while setting no restriction to the amount of sold energy. Self-sufficiency of degree f limits the amount of purchased energy to $1 - f$ of consumed energy.

Expressing self-sufficiency over a period of time allows for two different formulations. The first, called *average*, only ensures that the overall fraction of purchased energy is below the threshold

$$\sum_{t \in T} P_{\mathrm{demand},t} \cdot (1-f) \geq \sum_{t \in T} P_{\mathrm{buy},t}. \tag{3.32}$$

The second, called *individual*, ensures that at all individual time steps the threshold is not exceeded

$$P_{\mathrm{demand},t} \cdot (1-f) \geq P_{\mathrm{buy},t}. \tag{3.33}$$

3.3.3. Cyclic Storage Constraints

Components with storages contain variables describing the storage fill level at each step of the time series. The change from one step to the next is expressed by a discretised state equation. If no additional constraints are applied then the storage can be set to full capacity at the start of the time series and successively emptied instead of buying energy from the external grid, practically generating free energy. This exploitation can be prevented by enforcing that the storage has the same fill level in the beginning and the end of the time series, similar to [45, 60]. We introduce additional constraints for the biogas component

$$V_{\mathrm{biogas},T} = V_{\mathrm{biogas},0} \tag{3.34}$$

and each storage component $l \in L$

$$Q_{\mathrm{l},T} = Q_{\mathrm{l},0}. \tag{3.35}$$

4. Optimisation under Uncertainty

In this section, the MILP from Section 3 is extended to a two-stage stochastic program to account for uncertainty.

A two-stage stochastic program can be expressed by the form [42]

$$
\begin{aligned}
\min_{x,y_s}\ & F_{\mathrm{I}}(x) + \sum_{s \in S} \pi_s F_{\mathrm{II},s}(x, y_s) \\
\text{s.t.}\ & g_I(x) \geq 0 \\
& g_{\mathrm{II},s}(x, y_s) \geq 0.
\end{aligned}
\tag{4.1}
$$

The uncertainty in the parameters is represented by a set of scenarios S where each scenario $s \in S$ contains a value for each uncertain parameter. Each scenario also has a probability π_s. The decision variables are split into two stages. First stage variables x are decisions that have to be made before the uncertain values are known. The second stage, y_s, consists of decisions that can be delayed until the uncertainty is revealed. For each second stage variable one instance per scenario exists, index by scenario s, describing the decision made when the uncertain parameters take on the values of scenario s. Following the decision variables, the constraints are split into constraints depending only on first stage variables, $g_{\mathrm{I}}(x)$, and into constraints that also depend on second stage variables $g_{\mathrm{II,s}}(x, y_s)$, where one instance per scenario exists. The objective function is likewise split into an expression only depending on first stage variables $F_{\mathrm{I}}(x)$ and an expression that also depends on second stage variables $F_{\mathrm{II},s}(x, y_s)$. The second stage objective expressions are used to compute the expected objective value over all scenarios.

If the constraints and the objective function are linear functions, then we can express a two-stage stochastic problem as a LP. When certain variables are restricted to integer values, we get a MILP. In the case of two-stage stochastic programs, only small sized MILPs can be solved using conventional solvers and algorithms. For more complex problems special algorithms taking advantage of the two-stage formulation exist, like Bender Decomposition [8].

The number of uncertain parameters and scenarios are important factors in the development of two-stage stochastic problems. Increasing the number of parameters increases the complexity of the problem. However, failing to account for uncertainty in some parameters can lead to suboptimal design decisions [46]. The number of scenarios determines the accuracy of the uncertainty quantification, and therefore the accuracy of a solution. So a tradeoff between problem complexity, i.e., solving time and possible infeasibilities, on one side and accuracy and avoidance of suboptimal decisions on the other has to be struck. Additionally, the number of integer decisions on the second stage has to be kept to a minimum, due to the fact that for each integer decision one integer variable per scenario has to be introduced to the MILP, leading to large numbers of integer variables.

In the context of optimal DES design, first stage variables are called design variables, usually representing the installed capacities [41]. The second stage is called operation variables, representing operational decisions, like how much energy should be drawn from each storage component, or how much energy should be sold.

Section 4.1 details what parameters are considered uncertain. Section 4.2 extends the deterministic program from Section 3 into a two-stage stochastic program. Section 4.3 describes how the scenarios and their respective probabilities are calculated.

4.1. Uncertain Parameters

Each model parameter that is not considered to be uncertain can pose the risk leading to suboptimal design decision, while not increasing the complexity of the resulting problem. So a tradeoff between complexity and optimality has to be made. The additional goal of self-sufficiency also has to be considered.

The uncertain availability of renewable energy through photovoltaic and wind power create the biggest challenges in designing a renewable, self-sufficient energy system. The model parameter specifying solar availability is the specific capacity $p_{\text{pv},t}$, representing the fraction of the peak capacity that is available. The model parameter specifying wind availability is the specific capacity $p_{\text{wind},t}$, representing the available power from one wind turbine. Both parameters are viewed as uncertain for the optimisation of the DES.

Considering the goal of self-sufficiency, the energy demand that has to be met is an essential parameter. Influenced by many factors like population and industry behaviour, the energy demand cannot be known beforehand. Therefore, the model parameter $P_{\text{demand},t}$ representing the energy demand is also considered uncertain.

Further parameters that could be considered uncertain are electricity tariffs, feed in compensation, as well as costs of fuel and waste disposal. These factors can impact the economic performance of a given DES design. In this work, we do not consider them uncertain, but assume known values. This simplification is justified by the fact that we consider self-sufficiency as an additional design goal, which limits the amount of sold and purchased energy, reducing the impact of electricity tariffs and feed in compensation on the objective function.

4.2. Problem Extension

In the following the deterministic program from Section 3 is extended into a two-stage stochastic program.

The constraints and precomputations describing the power generation and energy storage components must be fulfilled for each scenario s.

Photovoltaic Component

$$0 \leq P_{\text{pv},s,t} \leq (P_{\text{pv,N,roof}} + P_{\text{pv,N,farm}}) \cdot p_{\text{pv},s,t} \tag{4.2}$$

$$p_{\text{pv},s,t} = \left(1 - \beta_{\text{ref}} \cdot \left(T_{\text{a},s,t} - T_{\text{ref}} + (T_{\text{NOCT}} - T_{\text{a},s,t}) \cdot \frac{G_{\text{T},s,t}}{G_{\text{NOCT}}}\right)\right) \cdot \frac{G_{\text{T},s,t}}{G_{\text{ref}}} \tag{4.3}$$

Wind Component

$$0 \leq P_{\mathrm{wind},s,t} \leq N_{\mathrm{wind}} \cdot p_{\mathrm{wind},s,t} \tag{4.4}$$

$$p_{\mathrm{wind},s,t} = 4\,\mathrm{MW} \cdot \eta_{\mathrm{wind}} \left(\frac{v_{\mathrm{wind,hub},s,t}}{10.205\,\mathrm{m/s}} \right) \tag{4.5}$$

$$v_{\mathrm{wind,hub,s,t}} = v_{\mathrm{wind},s,t} \cdot \frac{\ln(140\,\mathrm{m}/Z_0)}{\ln(H_{\mathrm{measure}}/Z_0)} \tag{4.6}$$

Biogas Component

$$0 \leq P_{\mathrm{biogas},s,t} \leq P_{\mathrm{biogas,N}} + P_{\mathrm{biogas,N,add}} \tag{4.7}$$

$$V_{\mathrm{biogas},s,t} = V_{\mathrm{biogas},s,t-1} + (P_{\mathrm{biogas,N}} \cdot 0.558\,\mathrm{m^3/kWh_e} - P_{\mathrm{biogas},s,t} \cdot 0.558\,\mathrm{m^3/kWh_e}) \cdot \Delta t \tag{4.8}$$

$$0 \leq V_{\mathrm{biogas},s,t} \leq V_{\mathrm{biogas,N}} \tag{4.9}$$

Hydroelectric Component

$$P_{\mathrm{hydro},s,t} = P_{\mathrm{hydro,N}} \tag{4.10}$$

Storage Components

$$0 \leq P_{\mathrm{l,char},s,t} \leq P_{\mathrm{l,char,N}} \tag{4.11}$$

$$0 \leq P_{\mathrm{l,dis},s,t} \leq P_{\mathrm{l,dis,N}} \tag{4.12}$$

$$Q_{\mathrm{l},s,t} = Q_{\mathrm{l},s,t-1} + (P_{\mathrm{l,char},s,t} \cdot \eta_{\mathrm{l,char}} - P_{\mathrm{l,dis},s,t} \cdot \eta_{\mathrm{l,dis}}^{-1}) \cdot \Delta t - Q_{\mathrm{l},s,t-1} \cdot \eta_{\mathrm{l,self}} \tag{4.13}$$

$$(1 - q_{\mathrm{l,max}}) \cdot Q_{\mathrm{l,N}} \leq Q_{\mathrm{l},s,t} \leq Q_{\mathrm{l,N}} \tag{4.14}$$

Consumption Component The energy demand of the city $P_{\mathrm{demand},s,t}$ is provided as time series of parameters for each scenario.

Grid Component The amount of purchased energy $P_{\mathrm{buy},s,t}$ and sold energy $P_{\mathrm{sell},s,t}$ are second stage variables.

Superstructure The energy balance of the local electricity grid is

$$\sum_{k\in K} P_{\mathrm{k},s,t} + \sum_{l\in L} P_{\mathrm{l,dis},s,t} + P_{\mathrm{buy},s,t} = \sum_{l\in L} P_{\mathrm{l,char},s,t} + P_{\mathrm{demand},s,t} + P_{\mathrm{sell},s,t}. \tag{4.15}$$

Objective Function The computations for the investment and maintenance costs for each component remain unchanged from the deterministic optimisation problem and are detailed in Section 2.

Unlike the investment and maintenance costs, the additional electricity costs depend on operational variables, meaning we have a different value for each scenario.

$$C_{\text{grid},s} = \sum_{t \in T} P_{\text{buy},s,t} \cdot c_{\text{buy}} \cdot \Delta t - P_{\text{sell},s,t} \cdot c_{\text{sell}} \cdot \Delta t. \tag{4.16}$$

The computations for the annualised investment costs, Equations (3.17) and (3.18), and total yearly maintenance costs, Equation (3.19), remain unchanged.

The additional costs from buying and selling energy is computed per scenario, so we calculate the expected additional costs

$$E(C) = \sum_{s \in S} \pi_s \cdot n_s \cdot C_{\text{grid},s} \tag{4.17}$$

using the individual probabilities π_s and weights n_s of each scenario. The weights n_s are used to adjust the time covered by scenario s. For the weights and probabilities see Section 4.3.2.

The objective function of the stochastic program remains unchanged from the deterministic one

$$TAC = I + M + E(C). \tag{4.18}$$

Capacity Limits The additional constraints enforcing capacity limitations, Equations (3.22) - (3.31), remain unchanged because they only restrict first stage variables.

Full self-sufficiency Considering full self-sufficiency, the deterministic program uses the feed in tariff and variables representing purchased energy to enforce full self-sufficiency while preventing possible infeasibilities. Both measures are adopted in the two-stage stochastic program. Allowing for curtailment in the solar and wind components is also adopted in the two-stage stochastic program, see Equations (3.2) and (3.4).

Partial self-sufficiency Regarding partial self-sufficiency, two possibilities exists to expand the individual and average strategies form the deterministic program into the stochastic program [45]. In the first, called *neutral*, the self-sufficiency strategy is enforced using the expected amount purchased and consumed energy over all scenarios. In the second, called *aggressive*, the strategy is enforced for each scenario individually.

This leads to three possible partial self-sufficiency strategies.

Average Neutral:

$$\sum_{s \in S} \left(\pi_s \cdot \sum_{t \in T} P_{\text{demand},s,t} \right) \cdot (1 - f) \geq \sum_{s \in S} \left(\pi_s \cdot \sum_{t \in T} P_{\text{buy},s,t} \right). \tag{4.19}$$

Average Aggressive:

$$\sum_{t\in T} P_{\text{demand},s,t} \cdot (1-f) \geq \sum_{t\in T} P_{\text{buy},s,t}. \tag{4.20}$$

Individual Aggressive:

$$P_{\text{demand},s,t} \cdot (1-f) \geq P_{\text{buy},s,t}. \tag{4.21}$$

The fourth possible strategy, Individual Neutral, is mathematically possible. However, limiting the expected amount of purchased energy to a set fraction of the expected amount of consumed energy for each time step individually would lead to a schedule that balances energy flows over all scenarios for each time step individually. Such scenario-spanning balances are contradictory to the time-spanning balances that are enforced using the average aggressive strategy and enabled via the storage components.

Cyclic Storage Constraints The cyclic storage constraints restrict operational variables and must therefore be fulfilled in each scenario

$$V_{\text{biogas},s,T} = V_{\text{biogas},s,0} \tag{4.22}$$

$$Q_{\text{l},s,T} = Q_{\text{l},s,0} \quad \forall l \in L. \tag{4.23}$$

This formulation has two consequences. First, storage operations are independent for each scenario. Storage fill levels and charging rates from one scenario do not impact other scenarios. When the underlying scenarios are a collection of typical periods representing a longer span of time, then they are temporally linked on each other. Such a dependence can not be represented by the above formulation of providing one copy of each second stage variable and constraint per scenario. Second, each storage can only operate in a cyclic manner over the length of the underlying time series.

Both consequences eliminate the possibility to model seasonal storages. Either the underlying time series has to span an entire year, which leads to infeasibly large optimisation problems, or the temporal dependence between different scenarios has to be incorporated into the problem formulations. Such an attempt to model seasonal storages exist [37, 25], but are beyond the scope of this work.

4.3. Scenario Generation

In this section the computation of a set of scenarios representing uncertainty in electric demand, and solar and wind availability is developed.

Mavromatidis et al. [46] review different methods to quantify the uncertainty of model parameters in DES design. The methodology of characterising the uncertainty varies from parameter to parameter. For demand uncertainty, two categories are observed, namely *total demand uncertainty* and *simulation-based demand uncertainty*.

In total demand uncertainty, simple probability distributions are extracted from historical data and future projections. These distributions are sampled to create sets of scenarios. If correlations between demand and other model parameters are considered, then they are implicitly handled by using historical data from the same source or explicitly when the probability distributions are calculated.

During simulation-based demand uncertainty models are employed that simulate the entity that creates the electricity demand. Usually building performance simulation (BPS) tools are used [46]. Multiple factors that influence the energy demands of a building are fed into a simulation software, which then simulates the building to generating demand profiles. Inputs include environmental factors like solar irradiation, occupancy behaviour like thermostat settings and architectural characteristics like building materials. Using the BPS tool, a large set of yearly scenarios is generated. Scenario reduction, like clustering extracted features [45], and aggregation, like k-medoids clustering to select typical days [19], are performed to reduce the size of resulting optimisation problem.

Uncertainty quantification for environmental parameters like wind speed or solar irradiation is most commonly done analogous to total demand uncertainty [46]. Probability density functions are fitted to measured data or data from a meteorological data base. Sometimes the data is divided into seasons, months or day night intervals to account for seasonal and diurnal variations. The fitted probability density function are then sampled to generate profiles. Similar to demand uncertainty, scenario reduction and aggregation can be performed to reduce the size of the problem formulation.

A third approach for demand uncertainty is used by Conejo et al. [15], where autoregressive moving average (ARMA) models are trained on historical data and then used to generate scenarios. Scenario reduction and aggregation is performed analogous to simulation-based demand uncertainty. This approach can also be used for environmental parameters. Correlation between model parameters can be considered implicitly, by handling historical data from the same source, or explicitly, by using cross correlation.

Using simulation-based demand uncertainty in the context of generating scenarios for a city is not applicable. The BPS tools used for yearly demand profile generation model a single building. In order to adapt this process for a smart city, each building in the city has to be modelled and simulated, which is not feasible.

Using ARMA models over total demand uncertainty has an advantage: The demand at a certain time step usually depends on the demand at previous time steps. This time dependent behaviour is build into ARMA models, where as it is lost during total demand uncertainty, because the distributions at each time step are sampled independently. Due to this advantage, an approach using ARMA models for both demand and environmental parameters is introduced in the following.

4.3.1. ARMA Model Based Demand Uncertainty

The uncertainty in a model parameter that changes over time, like electric demand, can be expressed as a time discrete stochastic process $Y = y_1 \dots y_k$, where for each time step t a random variable describes the stochastic nature of the parameter. Usually these random variables depend on each other, e.g., the electric demand at a certain time depends on the electric demand at previous time steps.

This behaviour of depending on past values can be captured using an ARMA model, which has the following form:

$$y_t = \sum_{j=1}^{p} \varphi_j \cdot y_{t-j} + \varepsilon_t - \sum_{j=1}^{q} \theta_j \cdot \varepsilon_{t-j}, \tag{4.24}$$

with autoregressive parameters $\varphi_1 \ldots \varphi_p$, moving average parameters $\theta_1 \ldots \theta_q$, and independent and identical normal distributed error terms $\varepsilon_1 \ldots \varepsilon_k \sim N(0, \sigma)$.

The autoregressive parameters express how much a value in the process depends on past values. The moving average parameters express how much a value in the process depends on past error terms. The error terms, and their distribution $N(0, \sigma)$, provide the stochastic behaviour found in the modelled stochastic process. The terms p and q are called the orders of the ARMA model.

In order for a stochastic process Y to be modelled by an ARMA model, two assumptions are made about the stochastic process. The normality assumption states that Y follows a normal distribution. The stationarity assumption states that the mean and variance of Y does not change over time. If a stochastic process fulfils both assumptions, an ARMA model can be trained by estimating the autoregressive and moving average parameters as well as the variance of the error term. Such a trained ARMA model can then be used to generate multiple realisations of the underlying stochastic process by sampling all error terms and using Equation (4.24) to compute the time series $y_1 \ldots y_k$. ARMA models can be extended to be more flexible dealing with time series that violate the stationary or normality assumptions, e.g., seasonal ARMA models can incorporate stationary violating cyclic patterns in a stochastic process. When finding the best fit ARMA model, or one of its extensions, the input stochastic process, has to be inspected for stationary and the orders of the ARMA model have to be picked. This can be accomplished using procedures like the Box-Jenkins method [10].

In our application of ARMA models for scenario generation, one model is trained per parameter. Correlations between the different parameters are implicitly handled by taking historical data from the same source. The three models then generate yearly demand and availability profiles. The remaining steps of scenario reduction and aggregation can be executed analogously to simulation-based demand uncertainty [46].

Using ARMA models presents new challenges. Detecting if a stochastic process is stationary and transforming it into a stationary one requires techniques from time series analysis. Additionally, the orders of the ARMA model have to be chosen carefully, either by using tools from time series analysis or training ARMA models with different orders and choosing the best fitting one. Finally training ARMA models on yearly profiles with hourly resolution is time consuming. Due to these factors, using ARMA model based demand uncertainty is not further pursued.

4.3.2. Total Demand Uncertainty

Deterministic demand profiles form the basis for computing scenarios using total demand uncertainty. These profiles are usually given as a set of typical periods, each typical period representing a set of actual periods within a year. Each typical period consists of one time series for each uncertain parameter. The goal is to compute multiple realisations of each typical period. If the input data is not given as a set of typical periods, then techniques like clustering can be used to determine typical periods. Then simple distributions are assigned to each time step and parameter within each typical period. The kind of distribution and its shape, like expected value or variance, depend on the parameter. The distributions are sampled to generate multiple realisations for each typical period, which can be used as scenarios for the stochastic program.

Determining typical periods Given a large time series based on historical data, determining typical periods is a form of scenario reduction. The historical data is split into periods, and reduction techniques are applied until a sufficiently small set of

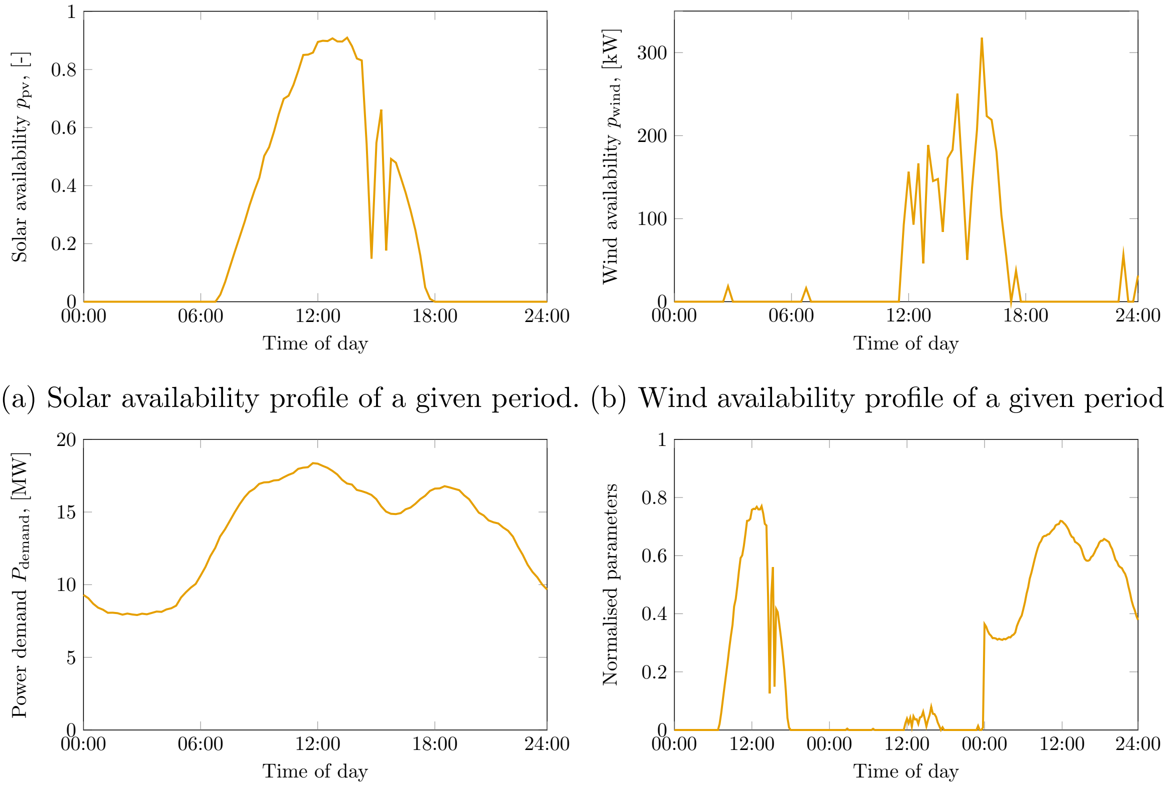

(a) Solar availability profile of a given period.

(b) Wind availability profile of a given period.

(c) Electric demand profile for a given period.

(d) Concatenated demand and availability profiles that represents a single period during clustering.

Figure 4.1: Time series concatenation.
Example to illustrate how multiple parallel running time series from a single period are combined. After each time series is normalised based on the maximum of the whole input time series, all time series are concatenated to form a single time series used during clustering.

periods remain. Such techniques can be clustering [19], based on distances between the time series of each period, or other methods based on probability distances [29].

Domínguez-Muñoz et al. [19] developed a method for determining typical periods for demand data of CHP systems. In the following, this approach is adopted to determine typical periods for electric demand, and solar and wind availability.

The input is one time series for each parameter. Each time series is normalised and then split into periods. For each period the values of all parameters are concatenated in order to calculate typical periods for all parameters at the same time, see Figure 4.1 for an example. Using k-medoid clustering, the periods are clustered into k clusters $C_1 \dots C_k$ represented by their medoid $c_1 \dots c_k$. The clustering is expressed in an MILP formulation.

The number of clusters k is determined by clustering for multiple values of k and choosing the clustering with the best quality, measured by two sets of indices. First the Davies-Bouding index I_{DB}, measuring the similarity within a cluster and the dissimilarity between different clusters. Second the error in load duration curve indices $ELDC_{\mathrm{pv}}$, $ELDC_{\mathrm{wind}}$, and $ELDC_{\mathrm{demand}}$, representing the error when reconstructing the load duration curve of each parameter using only the representative periods. Based on these indices the optimal clustering number and its clustering are chosen. The original time series of all typical periods are recovered by taking the cluster medoids and reversing the concatenation and normalisation.

Generating Scenarios After determining the typical periods using k-medoids clustering, the next step is to generate different realisations of each typical period. The naive approach is to assign simple distributions at each time step to the cluster medoid. However sampling these distributions loses time interdependent information between time steps and can introduce volatility into the resulting sampled time series. Additionally, just assigning distributions around the cluster medoid would disregard additional information contained within the cluster, see Figure 4.2 for an example.

We use an alternative approach, where uniformly members from each cluster are chosen to represent different realisations for each typical period, see Figure 4.2d. Choosing cluster members preserves the time interdependent information and does not introduce additional volatility into the set of computed realisations.

Given k cluster and m representatives per cluster, in the end $m \cdot k$ scenarios are computed.

Weights Scenarios originating from larger clusters represent more periods from the input time series, and therefore operational decisions that impact the objective function are more important and have to be weighted accordingly. Weights n_s for each scenario s are introduced into the objective function

$$n_s = \frac{n_{\mathrm{period}}}{\sum_{i=1}^{k} |C_i|} \cdot |C_{\mathsf{cluster}(s)}|, \tag{4.25}$$

where n_{period} is the number of periods that fit into a year, $|C_i|$ is the size of cluster i and $\mathsf{cluster}(s)$ is the assignment of scenario s to the cluster it originated from.

Probabilities Because each typical period is represented by m uniformly chosen cluster members, the probability of each scenario is set to

$$\pi_s = \frac{1}{m}. \tag{4.26}$$

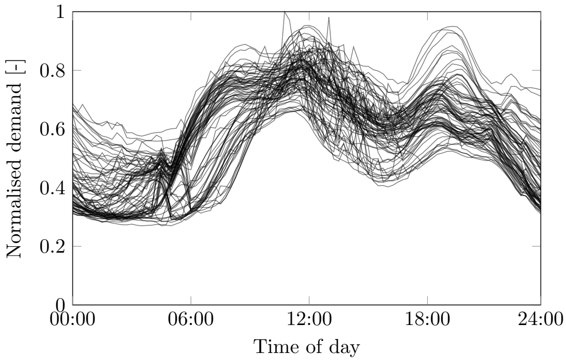

(a) Normalised demand profiles of all cluster members.

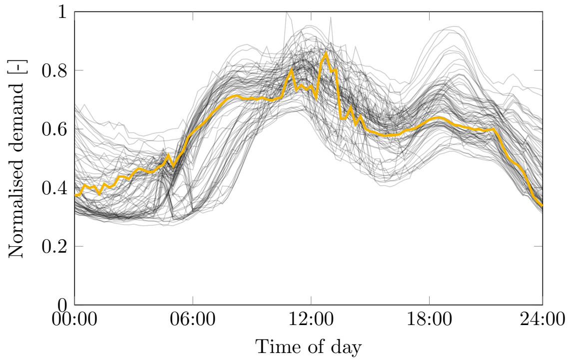

(b) Cluster medoid highlighted among all cluster members.

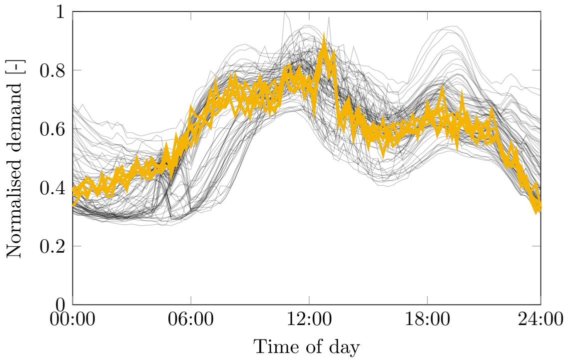

(c) Five realisations obtained from sampling of a normal distribution around the cluster medoid, where 95 % of the area under each distribution is between ± 20 % of the cluster medoid, based on [26].

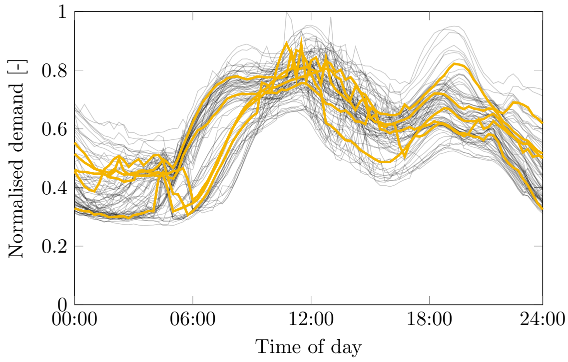

(d) Five realisation obtained from choosing 5 cluster member uniformly.

Figure 4.2: Time series sampling.
Examples illustrating the different approaches to generate multiple realisations of a given typical period. The cluster members and representatives are pictured by the black and yellow lines respectively. It is easy to see that the cluster is less volatile between 9 AM and 10 AM then between 12 PM and 2 PM. Additionally, the variance changes over time. Both variations are not represented in the five realisations from Figure (c) but represented within the five realisations from Figure (d).

Extreme events During clustering of time series, extreme events of peak demand or low availability can be excluded from the final set of scenarios. A DES designed based on an time series aggregated using clustering might not be able to operate during such extreme events. This necessitates the explicit handling of extreme events during time series aggregation [56]. In our case the extreme events are manually detected before aggregation and added to the final set of scenarios after clustering.

After splitting the input time series into periods, six extreme periods are selected, representing the highest or lowest sum of demand, or solar or wind availability. These six extreme periods are used to construct two extreme scenarios, but are not removed from the data set before clustering. In the first extreme scenario, the peak demand is combined with the low solar and wind availability. The second extreme scenario is constructed from the low demand and peak solar and wind availability periods. These extreme scenarios have to be included due to the design goal of full self-sufficiency, where no external grid is available to export excessive energy. Not including these extreme scenarios can lead to DES designs that are infeasible during the low demand and peak supply period due to excessive energy. The weights and probabilities of the extreme scenarios are set to zero, as suggested by Bahl et al. [7]. This eliminates the impact of operational decisions during the extreme scenarios on the objective function, but still guarantees that the resulting optimal DES design can feasibly operate during the extreme periods.

Length of a Typical Period The process described above can compute typical periods of different length. The length of a typical period during scenario generation can influence the performance of the optimal DES design based on the computed scenarios. Due to the cyclic storage constraints, see Section 3.3.3, each storage can only operate on a cyclic storage strategy over the length of the typical period. Usually typical days are used [45, 60]. Demand profiles however exhibit an additional weekly pattern, see Figure 4.3. Extending a typical period to a calender week, from Monday to Sunday, can increase the flexibility of possible storage strategies. However, extending period length form a day to a week reduces the number of periods available for clustering. So a tradeoff has to be made between possible storage flexibility and data availability when choosing period length. In Section 5, part of the case study discusses the effect of period length on storage schedules in optimal DES designs.

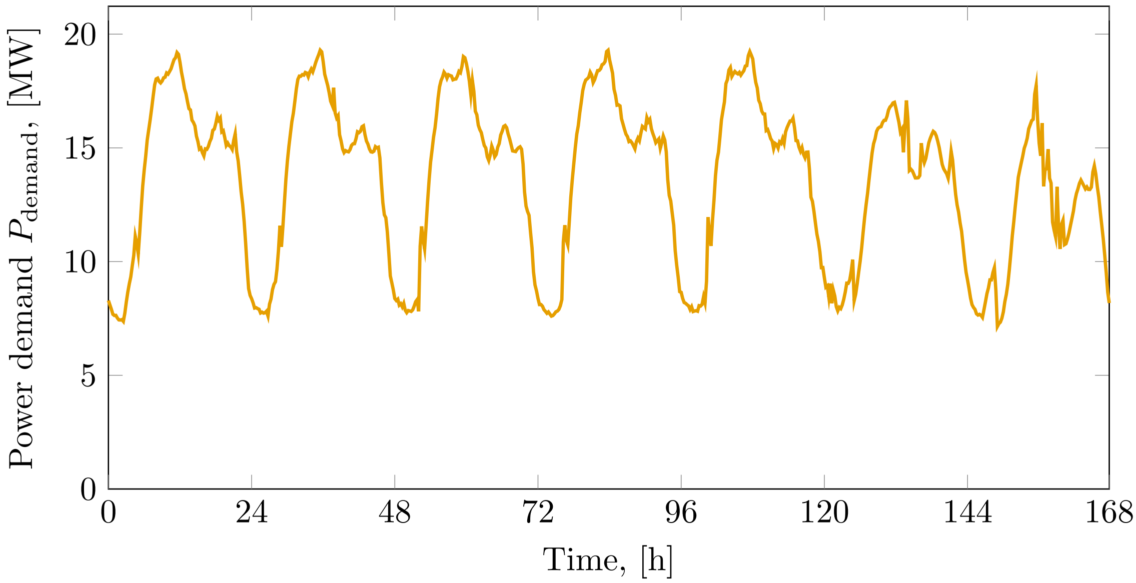

Figure 4.3: Weekly electric demand profile pattern.
Weekly demand profile of a given calender week, starting on Monday and ending on Sunday. The difference in the demand profile between weekdays and weekend days is visible.

5. Case Study

In this section, the MILP formulation from Section 4 is applied in a case study in two parts. In Section 5.1, the case study is set up and missing model parameters are specified. In the first part of the case study, Section 5.2, we investigate the influence of period length on storage schedules in optimal DES designs. In the second part, Section 5.3, we compare DES designs optimised for different levels of self-sufficiency.

5.1. Parameter Specifications and Problem Setup

In this section the case study is set up by providing the missing model parameters and historical data for the scenario generation. The case study is set up for Herzogenrath, a city in western Germany. The time frame spanned by the historical data ranges from the first Monday of 2016 to the last Sunday of 2018. This guarantees that the data can be split into a whole number of calender weeks. The model was formulated in the energy system modelling framework COMANDO [41], and solved using the Gurobi solver version 9.1.1 [27].

Solar and Wind Availability The meteorological data was provided by the Forschungszentrum Jülich [2], situated 22 km away from Herzogenrath. It provides the parameters G_{GHI} and v_{wind}, specifying solar irradiation and wind speed, respectively. Using the simplified computation from Appendix A.2, and Equation (4.2) and (4.4), the solar and wind availability parameters p_{pv} and p_{wind} are precomputed. The remaining values are listed in Table 5.1.

Parameter	Value	Source
Z_0	0.3 m	[13] [a]
H_{measure}	10 m	[2]
time zone	UTC+1 (MEZ)	[-]
latitude	50.90754	[-]
longitude	6.41121	[-]
$\theta_{\mathrm{T,array}}$	45°	[-]
$\theta_{\mathrm{A,array}}$	180°	[-]
β_{ref}	0.0034/°C	[23]
T_{ref}	25 °C	[23]
T_{NOCT}	45 °C	[23]
G_{ref}	1000 W/m^2	[23]

Table 5.1: Model parameters for the precomputation of solar and wind availability. The latitude and longitude describe the position of the Forschungszentrum Jülich, that provides the weather data, with UTC+1 being the local time zone. Daylight saving time was manually corrected in the meteorological and electric demand data. [a] Value taken for near-urban regions in Germany.

Electric Demand Electric demand data for Herzogenrath is provided by the enwor - energy & wasser vor ort GmbH [1], the local energy and water supplier of Herzogenrath. It represents the model parameter P_{demand}.

Technology Selection During the development of a model for the Hydrogen, PtG and Battery storage components, multiple technologies were considered. For the Hydrogen component, the Alkaline technology for electrolysis and PEM for fuel cells are selected, based on the combination with the lowest levelised cost of electricity [22]. Chemical methanisation is selected for the PtG component and Li-ion Batteries for the Battery component. Furthermore, Herzogenrath has no access to a river for a hydroelectric power plant or a possible site for pumped hydropower. The maximal capacities for both components are set to zero to reflect the inaccessibility.

Market Parameters The electricity price for purchasing electricity from the external grid c_{buy} is set to 150 €/MWh to penalise buying electricity, based on [17]. The feed-in tariff for selling electricity to the grid c_{sell} is set to half the average day-ahead market price for 2020: $0.5 \cdot 0.029\,52$ €/kWh $= 0.014\,76$ €/kWh [12].

Grid Shares To compare the scheduling of a given DES design and the impact of different components, their relative grid shares are computed, based on [45]. The grid shares are measured relative to the total energy consumption

$$TEC = \sum_{s \in S} \left(\pi_s \cdot n_s \cdot \sum_{t \in T} \left(\sum_{k \in K} P_{\text{k},s,t} + P_{\text{buy},s,t} \right) \right), \tag{5.1}$$

based on the purchased energy $P_{\text{buy},s,t}$ and the produced energy $P_{\text{k},s,t}$ of all production components $k \in K$.

The grid shares for production component $k \in K$ is

$$ES_k = \sum_{s \in S} \left(\pi_s \cdot n_s \cdot \sum_{t \in T} P_{\text{k},s,t} \right) / TEC. \tag{5.2}$$

The grid shares for purchased energy ES_{buy}, sold energy ES_{sell} and consumed energy ES_{demand} are computed analogously to Equation (5.2).

Due to the cyclic constraint for storage components, they do not consume or produce energy over the course of a scenario, except losses due to charging/discharging efficiencies and self-discharging. The amount of lost energy, and therefore the impact of each storage component on the grid shares can be computed by taking the difference between the energy charging into each storage unit and the energy discharging from it

$$ES_l = \sum_{s \in S} \left(\pi_s \cdot n_s \cdot \sum_{t \in T} P_{\text{l,char},s,t} - P_{\text{l,dis},s,t} \right) / TEC. \tag{5.3}$$

Scenario Representation Quality In order to assess the quality of the scenario representation, the annual sum of the uncertain parameters are computed. For the solar availability, p_{pv}, the annual energy potential AEP_{pv} represents the full-load hours per year. The annual energy potential is computed for the historical data and for each scenario representation. The historical data is given as a time series $p_{\text{pv},t}$ and the annual energy potential is computed by

$$AEP_{\text{pv}} = \sum_{t \in T} p_{\text{pv},t} \cdot \Delta_t \cdot \frac{1}{3}. \tag{5.4}$$

where the factor of three in the denominator compensates the fact, that the historical data consists of a three year period.

For a scenario representation $p_{\text{pv},s,t}$ the annual energy potential is computed by

$$AEP_{\text{pv}} = \sum_{s \in S} \left(\pi_s \cdot n_s \cdot \sum_{t \in T} p_{\text{pv},s,t} \cdot \Delta_t \right). \tag{5.5}$$

For the wind availability, p_{wind}, the annual energy potential AEP_{wind} represents the annual energy production of a single wind turbine. For the energy demand P_{demand}, the annual energy demand AED is used. Both values are computed analogous to Equation (5.4) and Equation (5.5).

5.2. Length of a Typical Period

In order to compare the influence of typical days and typical weeks, one set of scenarios is computed for each length from the same data set. For both cases, $m = 5$ representatives are picked from each cluster. Due to the focus on storage schedules, both optimal DES designs must contain energy storages. In Section 5.3, the effects of different enforcing strategies and self-sufficiency levels on DES designs are examined. The base case, with no self-sufficiency constrains does not utilize energy storages. The Average Neutral strategy with a self-sufficiency level $f = 0.5$ represent the most relaxed self-sufficiency that forces the DES to incorporate energy storages into its design. Therefore, the Average Neutral strategy with $f = 0.5$ is used to obtain DES designs with energy storages.

Scenario Generation for Days The data is split into 1092 days, and clustered using the approach discussed in Section 4.3.2. Based on the Davies-Bouding index, see Figure 5.1a, cluster numbers $k = \{2, 4, 6, 7\}$ are the most promising. Factoring in the error in load duration curve, Figure 5.1b, especially $ELDC_{\text{wind}}$, which exhibit a lower error at $k \geq 6$, $k = 6$ is the most optimal clustering number. Choosing $m = 5$ representatives per cluster and adding the two extreme scenarios results in $m \cdot k + 2 = 32$ scenarios. To compute the weights n_s, the number of periods fitting in a year n_{period} is set to 365. The probabilities π_s are set to $\frac{1}{m} = 0.2$.

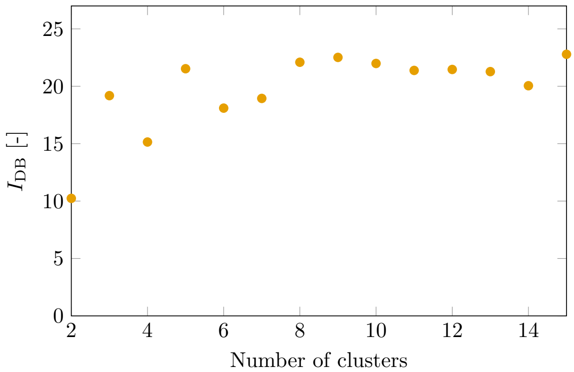

(a) The Davies-Bouding index I_{DB} measures the similarity within each cluster and the dissimilarity between different clusters for different number of clusters. The lower the index, the better the clustering.

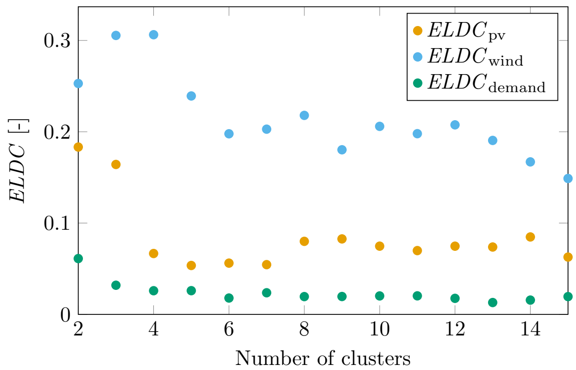

(b) The error in load duration curve indices $ELDC$ for each parameter for different number of clusters. The lower the indices, the better the clustering.

Figure 5.1: Indices used to decide optimal clustering number of typical days. The indices measure the accuracy of clustering the solar and wind availability and demand data into representative days. Based on them, the clustering with $k = 6$ clusters is chosen.

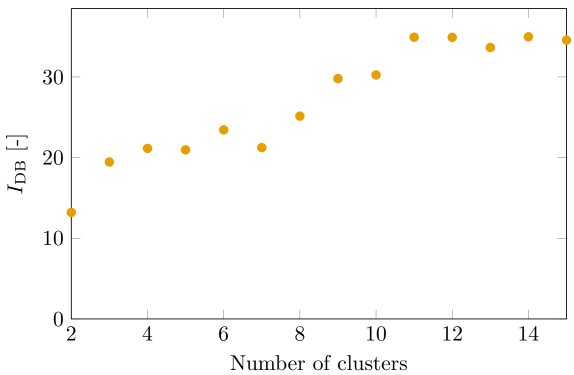

(a) The Davies-Bouding index I_{DB} measuring the similarity within each cluster and the dissimilarity between different clusters for different number of clusters. The lower the index, the better the clustering.

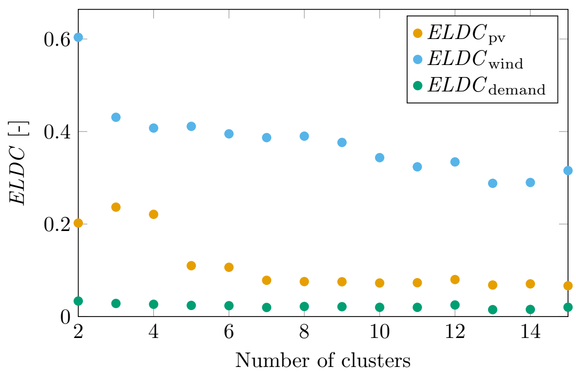

(b) The error in load duration curve indices $ELDC$ for each parameter for different number of clusters. The lower the indices, the better the clustering.

Figure 5.2: Indices used to decide optimal clustering number of typical days. The indices measure the accuracy of clustering the solar and wind availability and demand data into representative weeks. Based on them, the clustering with $k = 5$ clusters is chosen.

Scenario Generation for Weeks Analogous to the scenario generation for days, the data is split into 156 weeks and clustered. The cluster indices are shown in Figure 5.2. Based on the sharp decrease of $ELDC_{\text{pv}}$ between $k = 4$ and $k = 5$, $k = 5$ is the most promising cluster number. All other indices exhibit similar or increasing behaviour from $k = 5$ onward, therefore the clustering with $k = 5$ cluster is chosen. Representing each cluster with $m = 5$ scenarios and adding two extreme scenarios, results in $m \cdot k + 2 = 27$ scenarios. The number of periods fitting into a year n_{period} is set to $\frac{365}{7}$ and the probabilities π_s to $\frac{1}{m} = 0.2$.

Results With the two scenario sets computed above, two optimal DES designs are determined using the MILP formulation from Section 4. Figure 5.3 shows the capacities from the optimal DES designs for both scenario sets. Figure 5.4 shows the grid shares from both DES designs. All three available storage technologies (Hydrogen, PtG and Batteries) are not utilised in both DES designs. The flexible biogas component functions as the only energy storage.

Table 5.2 shows the annual energy potential and annual energy demand of the historical data as well as the two scenario representations. The values suggest that the week based design represents the historical data with a higher precision. Between the day based and week based scenario set, the indices exhibit large differences, especially AEP_{wind}, complicating the comparison of the storage strategies of the computed DES designs.

Comparing the capacities of both DES designs, the day based design uses more wind turbines. The decreased number of wind turbines in the week based design is compensated by a larger biogas capacity. The PV component is of similar size.

The storage volume in the biogas component is considerably bigger in the week based design. The amount of biogas generated is proportional to the biogas base capacity $P_{\text{biogas,N}}$, according to Equation (2.19). The increase in the amount of generated biogas is half of the increase in the base capacity, and so considerably smaller than the increase in the storage volume. This suggests that besides the larger amount of biogas generated, the storage volume is bigger because the gas is stored for a longer period of time, suggesting a higher utilisation of the storage.

Two explanations for the decrease in the wind component and the increase on the storage volume arise. In the first, the wind component is utilised less solely because of

Value	Historical Data	Typical Days	Typical Weeks
AEP_{pv}	1204.55 h	1239.73 h	1212.13 h
AEP_{wind}	4185.86 MWh	5285.40 MWh	3690.99 MWh
AED	137 286.84 MWh	140 002.03 MWh	137 723.58 MWh

Table 5.2: Annual energy potential and annual energy demand of the historical data and different scenario representations.
Overall the typical days representation deviates further away from the historical data than the weeks based representation.

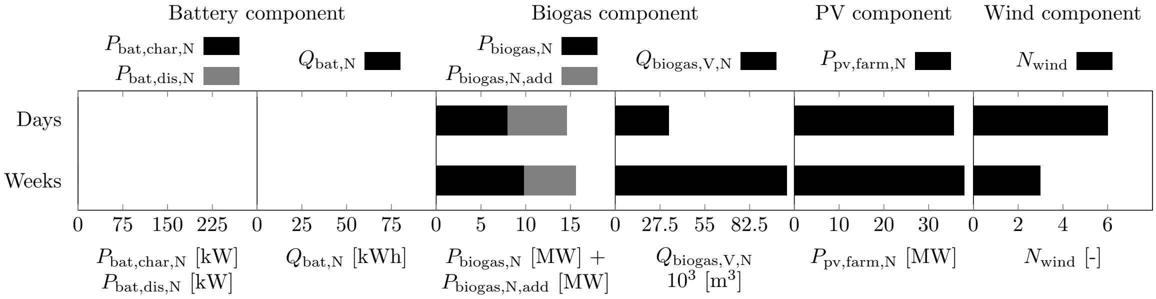

Figure 5.3: Capacities of optimal DES design based on different lengths of typical periods.
The capacities for the Hydrogen PtG and Battery components are zero for all DES designs.

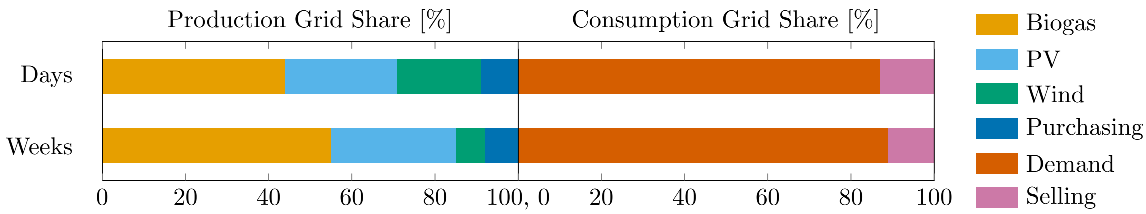

Figure 5.4: Grid shares of optimal DES designs based on different lengths of typical periods.

the smaller annual energy potential and the biogas storage is bigger solely because the time the gas is stored is longer. In the second, the annual energy potential has a larger impact on the size of the wind component, i.e. without an energy storage, the week based design would have eliminated the wind component. Additionally, the longer scenario length enables higher storage flexibility and higher utilisation of the wind component, explaining the larger storage volume. The overall effect is that the week based design utilised the wind component despite the smaller annual energy potential because the longer scenario length enables more utilisation of wind energy. The second explanation is supported by the fact that the PV component is utilised more in the week based design despite the week based scenario set having a smaller annual energy potential for the solar component.

More investigation is needed to conclude if longer typical period length increases storage flexibility and solar and wind power utilisation. The annual energy potential and annual energy demand indices suggest that the week based scenario set represent the historical data more accurately, but more dedicated investigation is needed.

5.3. Self-Sufficiency

In this part of the case study, optimal DES designs under different constraints of self-sufficiency are compared. In order to provide the most flexibility for the storage

Strategy	f
Base Case	-
Average Neutral	0.5
Average Neutral	0.9
Average Neutral	1
Average Aggressive	0.5
Average Aggressive	0.9
Average Aggressive	1
Individual Aggressive	0.5
Individual Aggressive	0.9
Individual Aggressive	1
Full Self-Sufficiency	-

Table 5.3: Combinations of enforcing strategies and self-sufficiency levels examined. During the base case, no additional constraints are added to the optimisation problem.

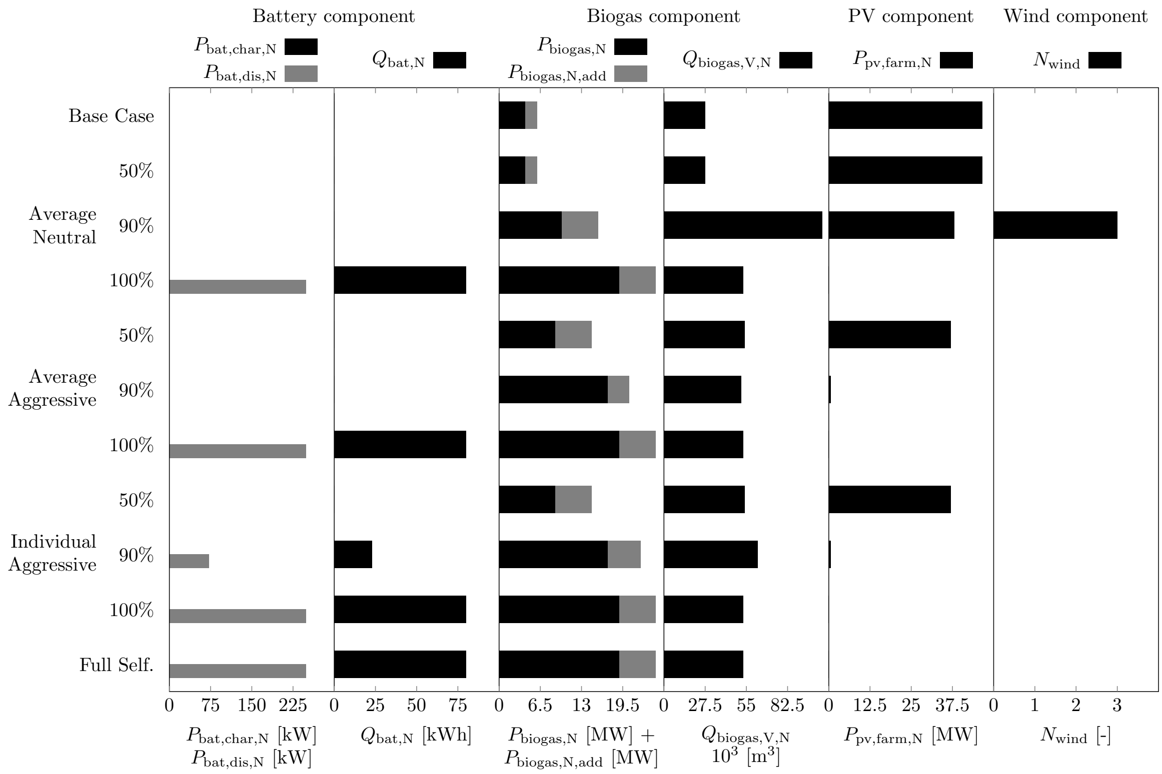

Figure 5.5: Capacities of optimal DES designs based on different combinations of enforcing strategies and levels of self-sufficiency.
The capacities for the Hydrogen and PtG components are zero for all DES designs. $P_{bat,char,N}$ are non zero for the DES designs that utilise the battery component, but are so small that they do not register on the graph.

components, the scenario set based on typical weeks is used in all model runs. All combinations of enforcing strategies and self-sufficiency levels examined are listed in Table 5.3. The exact formulations of each enforcing strategy are detailed in Section 4.2.

Results Figure 5.3 shows the capacities and Figure 5.4 shows the grid shares of the DES designs of all combinations of enforcing strategies and self-sufficiency levels examined. All DES designs that utilise dedicated energy storages use the battery storage component, but with so small capacities and grid shares that the effects on the DES schedule is insignificant. The capacities of the remaining storage components, hydrogen and PtG, are zero. In the remaining DES designs, the capacities of all three storage components are likewise zero. The flexible biogas component functions as the main storage.

Based on the capacities in Figure 5.5 and grid shares in Figure 5.6, the test cases exhibit a trend from less aggressive to more aggressive enforcing strategies and self-sufficiency levels. The capacities of the PV component decrease. The decrease of the PV capacities and the amount of purchasable energy due to higher levels of self-sufficiency is compensated by larger biogas capacities.

Overall, the Average Aggressive and Individual Aggressive strategies with the same self-sufficiency level result in similar DES designs. Between the Average Aggressive and the Average Neutral strategy, smaller biogas capacities and larger PV capacities can be observed in the later.

The base case and the Average Neutral 50 % case result in the same DES design, suggesting that the base case already purchases less than 50 % of the demand over all scenarios.

An anomaly is the Average Neutral 90 % case, which is the only test case with a non-zero wind component. It is also the only design with a considerably lager biogas storage volume, suggesting that the large volume became necessary with the large wind component, and not due to self-sufficiency.

Moving to the Average Aggressive and Individual Aggressive 90 % test cases, the PV component is scaled back considerably and the biogas component is scaled up. During scenarios with low availability, in order to not exceed the 10 % purchasing threshold, the biogas component has to be scaled up. The increased production capacity is then also utilized in scenarios with high solar availability, decreasing the size of the PV component.

The trend of decreasing solar capacities and increasing biogas capacities culminates in the extreme test cases of 100 % partial self-sufficiency and full self-sufficiency. Both test cases result in a similar design with no PV component and a scaled up biogas component. The biogas component has to handle a very large fraction of the energy demand during the extreme scenario with low availability and peak demand. The resulting large biogas capacity is then also able to handle all other scenarios, eliminating the need for solar and wind components.

The similar designs can be explained by the fact that the self-sufficiency constraints with $f = 1$ are mathematically equivalent. The only difference is between the three partial self-sufficiency strategies and the full self-sufficiency strategy is the feed-in tariff, which is zero for full self-sufficiency and 0.014 76 €/kWh for partial self-sufficiency.

Overall, moving from less aggressive enforcing strategies and lower self-sufficiency levels to more aggressive strategies with higher levels, a displacement of variable energy sources like solar and wind with reliable technologies can be observed. The central effect is that low availability scenarios force larger capacities in the biogas component, making PV and wind less necessary. This could be alleviated using seasonal storages, where energy can be transferred form high availability to low availability scenarios.

When looking at the different enforcing strategies, our results show that there is no difference between the Average Aggressive and Individual Aggressive strategies. The Average Neutral strategy however relaxes the self-sufficiency goal and enables for more energy to be purchased during low availability scenarios, when it can be compensated during other scenarios. However, when introducing seasonal storages using explicit formulations [37, 25], then energy purchases can be freely distributed across all scenarios given enough storage capacity. A design that fulfils the Average Neutral strategy without a seasonal storage could fulfil the same threshold in the Average Aggressive or even the Individual Aggressive strategy when a seasonal storage is installed, facilitating the incorporation of solar and wind energy under more extreme self-sufficiency targets.

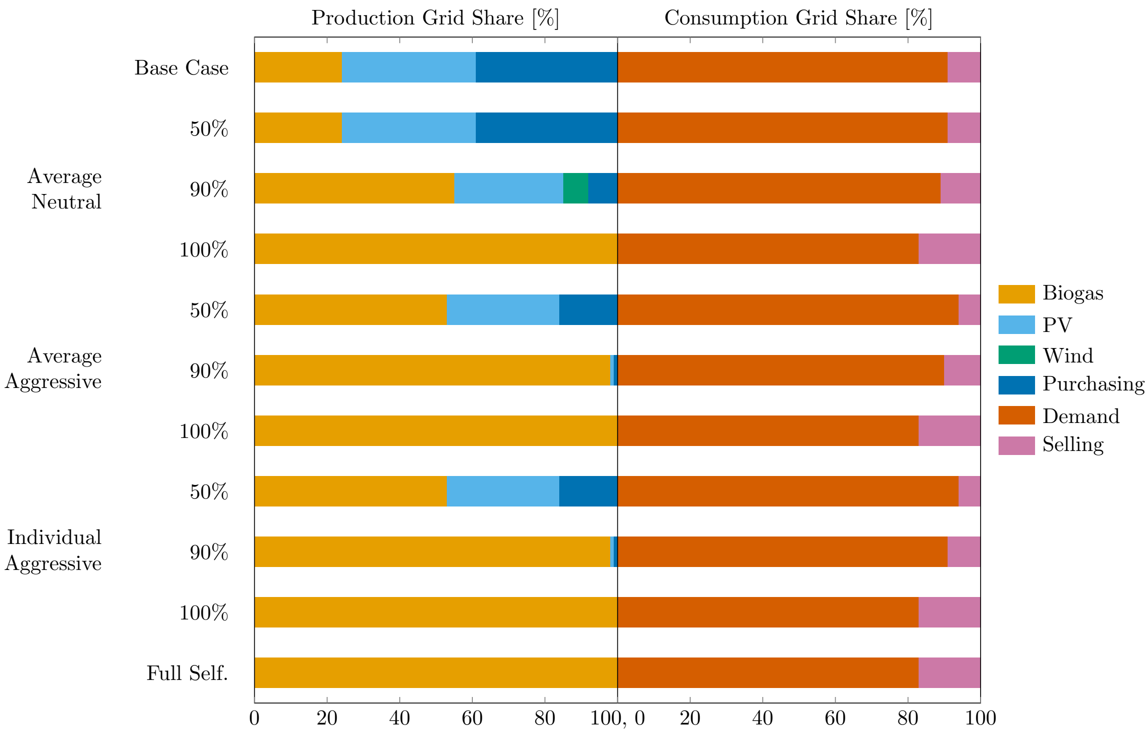

Figure 5.6: Grid shares of optimal DES designs based on different combinations of enforcing strategies and levels of self-sufficiency.
The grid shares of purchased energy are well below 0.1 percent and do not register on the graph. This also applies to the grid shares of the battery component for the DES designs that utilise the battery component.

6. Conclusion

In this work we developed a two-stage stochastic program to optimise DES designs for smart cities under constrains of self-sufficiency. The program considers solar and wind energy production and electric demand as uncertain. First a mathematical model describing the behaviour of a DES was presented. It incorporates four renewable energy technologies and four storage technologies. The model is then translated into an optimisation problem, expressed as an MILP, optimising the total annual cost of a DES design. Additional constraints enforcing self-sufficiency were added to the optimisation problem. Different enforcing strategies and self-sufficiency levels were presented.

Using a two-stage stochastic formulation, we extended the optimisation problem to handle uncertainty regarding model parameters. The electricity demand and solar and wind availability were considered uncertain. Three techniques for scenario generation for optimal DES design were discussed. Usually used in the context of designing DES for single buildings, the scenario generation techniques had to be adapted for the use in DES design for cities. Total demand uncertainty using typical periods was the most promising technique, yielding a scenario generation method based on aggregating historical data into typical periods. The process was adapted to work with typical periods of different length.

Using a case study of Herzogenrath, a city in western Germany, the two-stage stochastic program and the scenario generation methods were evaluated. We examined effects of aggregating historical data into typical days or typical weeks during scenario generation on the resulting optimal DES designs. Longer typical periods seem to increase the flexibility in the DES operating schedule regarding storage components. We also examined the effects of different self-sufficiency enforcing strategies and different levels of self-sufficiency on optimal DES designs. With more aggressive strategies and higher levels of self-sufficiency, a displacement of varying and uncertain energy source like solar and wind with stable and deterministic ones, like biogas, was observed.

Future Work In the first part of the case study we analysed the impact of typical period length on storage schedules in optimal DES designs. During analysis we observed that the scenario set based on longer typical periods more accurately reflects the historical data. Further investigations on the accuracy of the scenario representations are needed. Additionally, further investigations are needed to conclude if longer typical periods increase storage flexibility and utilisation of uncertain energy sources like solar and wind. During the second part of the case study, we suspect that seasonal storages could lead to higher utilization of varying and uncertain energy sources under more extreme constraints of self-sufficiency. The effects of incorporating seasonal storages into the model and problem formulation should be examined in future works.

During scenario generation, historical data is used as a basis for quantifying the uncertainty of electricity demand. Future trends like the widespread adoption of electric vehicles could impact the energy demand profile in unpredictable ways. Only relying on historical data when generating scenarios does not account for such external factors.

The scenario generation can also be extended to include more model parameters, like energy prices and their projected changes in the future.

The model of the DES used in this work was designed for cities, but can also be used to develop larger DES for metropolitan areas or larger regions.

Our model assumes that all energy producing and storing facilities have to be built from scratch. However, renewable energy infrastructure is already installed in many cities. Extending the model to make it possible to incorporate existing energy producing and storing infrastructure can ease the application of the model for cities with preexisting infrastructure.

References

[1] enwor - energie & wasser vor ort GmbH, Herzogenrath.

[2] Forschungszentrum Jülich GmbH, Geschäftsbereich Sicherheit und Strahlenschutz - Umwelt - Meteorologie, Jülich.

[3] Commercialisation of energy storage in Europe. Technical report, Fuel Cells and Hydrogen Joint Undertaking, 2015.

[4] The future cost of electricity-based synthetic fuels. Technical report, Agora Verkehrswende, Agora Energiewende and Frontier Economics, 2018.

[5] Kaveh Akbari, Mohammad Mahdi Nasiri, Fariborz Jolai, and Seyed Farid Ghaderi. Optimal investment and unit sizing of distributed energy systems under uncertainty: A robust optimization approach. *Energy and Buildings*, 85:275–286, 2014.

[6] Kaveh Akbari, Fariborz Jolai, and Seyed Farid Ghaderi. Optimal design of distributed energy system in a neighborhood under uncertainty. *Energy*, 116:567–582, 2016.

[7] Björn Bahl, Alexander Kümpel, Hagen Seele, Matthias Lampe, and André Bardow. Time-series aggregation for synthesis problems by bounding error in the objective function. *Energy*, 135:900–912, 2017.

[8] J Benders. Partitioning procedures for solving mixed-variables programming problems. *Numerische mathematik*, 4(1):238–252, 1962.

[9] John R Birge and Francois Louveaux. *Introduction to stochastic programming.* Springer Science & Business Media, 2011.

[10] George EP Box, Gwilym M Jenkins, Gregory C Reinsel, and Greta M Ljung. *Time series analysis: Forecasting and control.* John Wiley & Sons, 2015.

[11] Deutscher Bundestag. Bundestag ändert das Erneuerbare-Energien-Gesetz. `https://www.bundestag.de/dokumente/textarchiv/2020/kw51-de-erneuerbare-energien-gesetz-812876`, 2020. accessed 18-10-2020.

[12] Bruno Burger. Nettostromerzeugung in Deutschland im Jahr 2020. `https://energy-charts.info/post.html?l=de&c=DE&q=nettostromerzeugung_in_deutschland_im_jahr_2020_01022021`, 2021. accessed 27-04-2021.

[13] Jürgen Christoffer and Monika Ulbricht-Eissing. *Die bodennahen Windverhältnisse in der Bundesrepublik Deutschland.* Dt. Wetterdienst, Zentralamt, 1989.

[14] European Commision. Factsheet: The revised renewable energy directive. `https://ec.europa.eu/energy/sites/ener/files/documents/directive_renewable_factsheet.pdf`, 2019. accessed 18-10-2020.

[15] Antonio J Conejo, Miguel Carrión, Juan M Morales, et al. *Decision making under uncertainty in electricity markets*, volume 1. Springer, 2010.

[16] Jochen Conrad, Christoph Pellinger, and Michael Hinterstocker. Gutachten zur Rentabilität von Pumpspeicherkraftwerken. Technical report, Forschungsstelle für Energiewirtschaft eV, 2014.

[17] Giancarlo Dalle Ave, Iiro Harjunkoski, and Sebastian Engell. A non-uniform grid approach for scheduling considering electricity load tracking and future load prediction. *Computers & Chemical Engineering*, 129, 2019.

[18] Marialaura Di Somma, Giorgio Graditi, Ehsan Heydarian-Forushani, Miadreza Shafie-khah, and Pierluigi Siano. Stochastic optimal scheduling of distributed energy resources with renewables considering economic and environmental aspects. *Renewable energy*, 116:272–287, 2018.

[19] Fernando Domínguez-Muñoz, José M Cejudo-López, Antonio Carrillo-Andrés, and Manuel Gallardo-Salazar. Selection of typical demand days for CHP optimization. *Energy and buildings*, 43(11):3036–3043, 2011.

[20] 100% Renewable Energy. Windatlas. `http://windatlas.xyz/turbines`. accessed 11-01-2021.

[21] Fachagentur Nachwachsende Rohstoffe eV. Flexibilisierung von Biogasanlagen. `https://fnr.de/fileadmin/allgemein/pdf/broschueren/Broschuere_Flexibilisierung_Biogas_Web.pdf`, 2018. accessed 18-10-2020.

[22] Domenico Ferrero, Martina Gamba, Andrea Lanzini, and Massimo Santarelli. Power-to-Gas hydrogen: Techno-economic assessment of processes towards a multi-purpose energy carrier. *Energy Procedia*, 101:50–57, 2016.

[23] *First Solar Series 4 PV Module*. First Solar, 2015.

[24] Fraunhofer Institute for Solar Energy Systems. Photovoltaics report. `https://www.ise.fraunhofer.de/content/dam/ise/de/documents/publications/studies/Photovoltaics-Report.pdf`, 2020. accessed 18-10-2020.

[25] Paolo Gabrielli, Matteo Gazzani, Emanuele Martelli, and Marco Mazzotti. Optimal design of multi-energy systems with seasonal storage. *Applied Energy*, 219: 408–424, 2018.

[26] Satoshi Gamou, Ryohei Yokoyama, and Koichi Ito. Optimal unit sizing of cogeneration systems in consideration of uncertain energy demands as continuous random variables. *Energy Conversion and Management*, 43(9-12):1349–1361, 2002.

[27] LLC Gurobi Optimization. Gurobi optimizer reference manual. `http://www.gurobi.com`, 2021. accessed 11-02-2021.

[28] Niklas Hartmann, Ludger Eltrop, Nikolaus Bauer, Johannes Salzer, Simon Schwarz, and Maike Schmidt. Stromspeicherpotenziale für Deutschland. Technical report, Universität Stuttgart, 2012.

[29] Holger Heitsch and Werner Römisch. Scenario reduction algorithms in stochastic programming. *Computational optimization and applications*, 24(2):187–206, 2003.

[30] Michelle Hofer. Kostenanalyse von Laufwasserkraftwerken in Europa. Master's thesis, Graz University of Technology, 2018.

[31] Frank P. Incorpera. *Consequences of global warming*, pages 80–107. Cambridge University Press, 2015.

[32] Verena Jülch, Jessica Thomsen, Niklas Hartmann, Tobias Junne, Lea Unterreiner, Markus Arnold, Sören Reith, Ludger Eltrop, Sandra Wassermann, and Marlen Niederberger. Betreibermodelle für Stromspeicher–ökonomisch-ökologische Analyse und Vergleich von Speichern in autonomen, dezentralen Netzen und für regionale und überregionale Versorgungsaufgaben. Technical report, Fraunhofer-Institut für Solare Energiesysteme, Universität Stuttgart Institut für Energiewirtschaft und rationelle Energieanwendung, TTI GmbH/TGU Compare Consulting, 2016.

[33] Ehsanul Kabir, Pawan Kumar, Sandeep Kumar, Adedeji Adelodun, and Ki-Hyun Kim. Solar energy: Potential and future prospects. *Renewable and Sustainable Energy Reviews*, 82, 2017.

[34] Fritz Kasten and Andrew T Young. Revised optical air mass tables and approximation formula. *Applied optics*, 28(22):4735–4738, 1989.

[35] Greg Kopp and Judith L Lean. A new, lower value of total solar irradiance: Evidence and climate significance. *Geophysical Research Letters*, 38(1), 2011.

[36] Christoph Kost, Shivenes Shammugam, Verena Jülch, Huyen-tran Nguyen, and Thomas Schlegl. Stromgestehungskosten Erneuerbare Energien. Technical report, Fraunhofer Institute for Solar Energy Systems, 2018.

[37] Leander Kotzur, Peter Markewitz, Martin Robinius, and Detlef Stolten. Time series aggregation for energy system design: Modeling seasonal storage. *Applied energy*, 213:123–135, 2018.

[38] Sandia National Laboratories. Angle of incidence. `https://pvpmc.sandia.gov/modeling-steps/1-weather-design-inputs/plane-of-array-poa-irradiance/calculating-poa-irradiance/angle-of-incidence/`, . accessed 18-10-2020.

[39] Sandia National Laboratories. POA ground reflected. `https://pvpmc.sandia.gov/modeling-steps/1-weather-design-inputs/`

plane-of-array-poa-irradiance/calculating-poa-irradiance/poa-ground-reflected/, . accessed 18-10-2020.

[40] Global Monitoring Laboratory. NOAA Solar Calculater. https://www.esrl.noaa.gov/gmd/grad/solcalc/calcdetails.html. accessed 18-10-2020.

[41] Marco Langiu, David Yang Shu, Florian Joseph Baader, Dominik Hering, Uwe Bau, Adre Xhonneux, Dirk Müller, Andre Bardow, Alexander Mitsos, and Manuel Damen. COMANDO: A next-generation open-source framework for energy systems optimization. *Computer & Chemical Engineering*, 2021.

[42] Marco Locatelli and Fabio Schoen. *Global optimization: Theory, algorithms, and applications*. SIAM, 2013.

[43] Silke Lüers, Anna-Kathrin Wallasch, and Knud Rehfeldt. Kostensituation der Windenergie an Land in Deutschland–Update. Technical report, Deutsche WindGuard GmbH im Auftrag von BWE und VDMA. Varel, 2015.

[44] Carlos Marino, Md Abdul Quddus, Mohammad Marufuzzaman, Mark Cowan, and Amy E Bednar. A chance-constrained two-stage stochastic programming model for reliable microgrid operations under power demand uncertainty. *Sustainable Energy, Grids and Networks*, 13:66–77, 2018.

[45] Georgios Mavromatidis, Kristina Orehounig, and Jan Carmeliet. Design of distributed energy systems under uncertainty: A two-stage stochastic programming approach. *Applied energy*, 222:932–950, 2018.

[46] Georgios Mavromatidis, Kristina Orehounig, and Jan Carmeliet. A review of uncertainty characterisation approaches for the optimal design of distributed energy systems. *Renewable and Sustainable Energy Reviews*, 88:258–277, 2018.

[47] Georgios Mavromatidis, Kristina Orehounig, and Jan Carmeliet. Uncertainty and global sensitivity analysis for the optimal design of distributed energy systems. *Applied Energy*, 214:219–238, 2018.

[48] Peter McKendry. Overview of anaerobic digestion and power and gas to grid plant capex and opex costs. *International Journal of Bioprocessing and Biotechniques*, 2019.

[49] Klima und Energiewirtschaft Baden-Württemberg Ministerium für Umwelt. Freiflächensolaranlagen Handlungsleitfaden. https://www.hamburg-institut.com/images/pdf/studien/Handlungsleitfaden_Freiflaechensolaranlagen.pdf, 2019. accessed 18-10-2020.

[50] Richard Perez, Pierre Ineichen, Robert Seals, Joseph Michalsky, and Ronald Stewart. Modeling daylight availability and irradiance components from direct and global irradiance. *Solar energy*, 44(5):271–289, 1990.

[51] Derall M Riley, Jiashen Tian, Gamze Güngör-Demirci, Patrick Phelan, J Rene Villalobos, and Ryan J Milcarek. Techno-Economic assessment of CHP systems in wastewater treatment plants. *Environments*, 7(10):74, 2020.

[52] Hannah Ritchie. Sector by sector: Where do global greenhouse gas emissions come from? `https://ourworldindata.org/ghg-emissions-by-sector`, 2020. accessed 18-10-2020.

[53] Hannah Ritchie and Max Roser. CO2 emissions. `https://ourworldindata.org/co2-emissions`, 2020. accessed 18-10-2020.

[54] Peter Scholes and Esther Areikin. A survey of the UK anaerobic digestion industry in 2013. Technical report, Waste Resources Action Programme WRAP, UK, 2014.

[55] Elisa Skoplaki and John A Palyvos. On the temperature dependence of photovoltaic module electrical performance: A review of efficiency/power correlations. *Solar energy*, 83(5):614–624, 2009.

[56] Holger Teichgraeber, Constantin P Lindenmeyer, Nils Baumgärtner, Leander Kotzur, Detlef Stolten, Martin Robinius, André Bardow, and Adam R Brandt. Extreme events in time series aggregation: A case study for optimal residential energy supply systems. *Applied Energy*, 275:115223, 2020.

[57] Charlotte Van Leeuwen and Andreas Zauner. D8.3 Report on the costs involved with PtG technologies and their potentials across the EU. Technical report, Store and Go, 2018.

[58] Meng Wang, Hang Yu, Xiaoyu Lin, Rui Jing, Fangjun He, and Chaoen Li. Comparing stochastic programming with posteriori approach for multi-objective optimization of distributed energy systems under uncertainty. *Energy*, 210:118571, 2020.

[59] Harry Wirth and Karin Schneider. Aktuelle Fakten zur Photovoltaik in Deutschland. Technical report, Fraunhofer Institute for Solar Energy Systems, 2020.

[60] Yun Yang, Shijie Zhang, and Yunhan Xiao. Optimal design of distributed energy resource systems based on two-stage stochastic programming. *Applied Thermal Engineering*, 110:1358–1370, 2017.

List of Figures

List of Tables

A. Appendix

In this appendix, the equations for the computations of the total solar irradiance G_T are presented. The angle of incidence has to be considered in order to account for the cosine effect, see Section A.1. The computation of the total solar irradiation depends on the irradiation values measured by the weather station. If global horizontal irradiance and horizontal diffuse irradiance are measured, the extended computation in Section A.2 can be used. If only the global horizontal irradiance is measured, a simplified model can be considered, see Section A.3.

A.1. Angle of Incidence

In order to compute the angle in incidence, the position of the sun and the PV module mounting have to be considered. It is assumed that all PV modules are mounted in the same fixed orientation, with a tilt angle $\theta_{\mathrm{T,array}}$ from the horizontal and an azimuth angle $\theta_{\mathrm{A,array}}$ in degrees east from north. The sun zenith angle θ_Z and azimuth angle θ_A are computed from the time of day, day in the year and PV location, using the NOAA Solar Position Calculator [40]. Using the angles above, the angle of incident θ, between a ray of the sun and normal the surface of the PV module, can be computed by

$$\theta = \cos^{-1}(\cos(\theta_\mathrm{Z}) \cdot \cos(\theta_{\mathrm{T,array}}) + \sin(\theta_\mathrm{Z}) \cdot \sin(\theta_{\mathrm{T,array}}) \cdot \cos(\theta_\mathrm{A} - \theta_{\mathrm{A,array}})) \tag{A.1}$$

as suggested by [38].

A.2. Total Solar Irradiation

The computation of the total solar irradiation presented in this subsection uses the global horizontal irradiance and horizontal diffuse irradiance as input values. If only the global horizontal irradiance is given, the computation in Section A.3 can be used. The total solar irradiation G_T on a PV module consists of three components, the direct irradiation G_{direct}, diffuse irradiation G_{diffuse} and reflected irradiation $G_{\mathrm{reflected}}$

$$G_\mathrm{T} = G_{\mathrm{direct}} + G_{\mathrm{diffuse}} + G_{\mathrm{reflected}}. \tag{A.2}$$

The direct irradiation depends on the direct normal irradiance G_{DNI}, the solar radiation from the solar disc on a surface normal to the direction of the sun,

$$G_{\mathrm{direct}} = G_{\mathrm{DNI}} \cdot \cos(\theta). \tag{A.3}$$

If the direct normal irradiance is not provided, it can be computed from the global horizontal irradiation G_{GHI} and the diffuse horizontal irradiation G_{DHI}

$$G_{\mathrm{DNI}} = \frac{G_{\mathrm{GHI}} - G_{\mathrm{DHI}}}{cos(\theta_\mathrm{Z})}. \tag{A.4}$$

For the diffuse irradiation, the Perez model of diffuse irradiation on a tilted surface is used [50]. As input, it takes the diffuse horizontal irradiation G_{DHI}, the radiation from the sky excluding the solar disc on a horizontal plane. The model takes into account sky clearness ϵ

$$\epsilon = \frac{\frac{G_{\text{DHI}}+G_{\text{DNI}}}{G_{\text{DHI}}} + \kappa \cdot \theta_{\text{Z}}^3}{1 + \kappa \cdot \theta_{\text{Z}}^3}, \tag{A.5}$$

with constant $\kappa = 0.000005525$ for angles given in degrees and sky brightness Δ

$$\Delta = \frac{G_{\text{DHI}} \cdot AM}{E}, \tag{A.6}$$

with air mass AM and extraterrestrial irradiation $E = 1361\,\text{W/m}^2$ [35]. The air mass can be calculated using an approximation from Kasten and Young [34]

$$AM = \left(\cos(\theta_{\text{Z}}) + 0.50572 \cdot (96.07995 - \theta_{\text{Z}})^{-1.6364}\right)^{-1}. \tag{A.7}$$

The diffuse irradiation is correlated from the diffuse horizontal irradiation and the sky clearness and brightness using the following equations and coefficients from Table A.1.

$$G_{\text{diffuse}} = G_{\text{DHI}} \cdot \left((1 - F_1) \cdot \frac{1 + \cos(\theta_{\text{T,array}})}{2} + F_1 \cdot \frac{a}{b} + F_2 \cdot \sin(\theta_{\text{T,array}})\right). \tag{A.8}$$

$$F_1 = \max(0, f_{11} + f_{12} \cdot \Delta + f_{13} \cdot \theta_{\text{Z}}). \tag{A.9}$$

$$F_2 = f_{21} + f_{22} \cdot \Delta + f_{23} \cdot \theta_{\text{Z}}. \tag{A.10}$$

$$a = \max(0, \cos\theta). \tag{A.11}$$

$$b = \max(0.087, \cos(\theta_{\text{Z}})). \tag{A.12}$$

For the reflected irradiation, it is assumed that the module is in an idealised environment [39]. The irradiance on the infinite flat ground is uniform and equal to the global horizontal irradiation G_{GHI}, the radiation from the entire sky on a horizontal surface. The ground reflects diffusely, and with a reflectance of ρ. The reflected irradiation can then be computed by

$$G_{\text{reflected}} = G_{\text{GHI}} \cdot \rho \cdot \frac{1 - \cos(\theta_{\text{T,array}})}{2}. \tag{A.13}$$

Sky clearness	f_{11}	f_{12}	f_{13}	f_{21}	f_{22}	f_{23}
$1 \leq \epsilon < 1.065$	-0.8	0.588	-0.062	-0.06	0.072	-0.022
$1.065 \leq \epsilon < 1.23$	0.13	0.683	-0.151	-0.019	0.066	-0.029
$1.23 \leq \epsilon < 1.5$	0.33	0.487	-0.221	0.055	-0.064	-0.026
$1.5 \leq \epsilon < 1.95$	0.568	0.187	-0.295	0.109	-0.152	-0.014
$1.95 \leq \epsilon < 2.8$	0.873	-0.392	-0.362	0.226	-0.462	0.001
$2.8 \leq \epsilon < 4.5$	1.132	-1.237	-0.412	0.288	-0.823	0.056
$4.5 \leq \epsilon < 6.2$	1.06	-1.6	-0.359	0.264	-0.127	0.131
$6.2 \leq \epsilon$	0.678	-0.327	-0.25	0.156	-1.377	0.251

Table A.1: Coefficients used in the Perez model of diffuse radiation on a tilted surface based on sky clearness ϵ.

A.3. Simplified Computation

The computation of the total solar irradiation presented in this subsection uses the global horizontal irradiance as its input. If additionally the diffuse horizontal irradiance is available, the computation in Section A.2 should be used. The total solar irradiation G_T on a PV module consists only on the direct irradiation G_direct

$$G_\mathrm{T} = G_\mathrm{direct}. \tag{A.14}$$

The direct irradiation depends on the direct normal irradiance G_DNI, the solar radiation from the solar disc on a surface normal to the direction of the sun,

$$G_\mathrm{direct} = G_\mathrm{DNI} \cdot \cos(\theta). \tag{A.15}$$

The direct normal irradiance can be approximated from the global horizontal irradiation G_GHI, the radiation from the entire sky on a horizontal surface,

$$G_\mathrm{DNI} = \frac{G_\mathrm{GHI}}{cos(\theta_\mathrm{Z})}. \tag{A.16}$$